The Swift–Hohenberg equation with a nonlocal nonlinearity

David Morgan and Jonathan H. P. Dawes

Department of Mathematical Sciences, University of Bath,
Claverton Down, Bath BA2 7AY, UK

25th December 2013

Abstract

It is well known that aspects of the formation of localised states in a one-dimensional Swift–Hohenberg equation can be described by Ginzburg–Landau-type envelope equations. This paper extends these multiple scales analyses to cases where an additional nonlinear integral term, in the form of a convolution, is present. The presence of a kernel function introduces a new lengthscale into the problem, and this results in additional complexity in both the derivation of envelope equations and in the bifurcation structure.

When the kernel is short-range, weakly nonlinear analysis results in envelope equations of standard type but whose coefficients are modified in complicated ways by the nonlinear nonlocal term. Nevertheless, these computations can be formulated quite generally in terms of properties of the Fourier transform of the kernel function. When the lengthscale associated with the kernel is longer, our method leads naturally to the derivation of two different, novel, envelope equations that describe aspects of the dynamics in these new regimes. The first of these contains additional bifurcations, and unexpected loops in the bifurcation diagram. The second of these captures the stretched-out nature of the homoclinic snaking curves that arises due to the nonlocal term.

1 Introduction

Motivated by fluid mechanics, reaction-diffusion chemistry, and biological systems, pattern forming nonequilibrium systems continue to attract significant research interest [16, 10]. They form a broad class of dissipative continuum nonlinear systems that describe important processes in nature. It is well known that pattern forming, or Turing, instabilities can give rise to solution branches corresponding to regular spatial structures [11], which typically emerge from a bifurcation point as a system parameter is varied. In some cases one observes localised patches of pattern rather than regular structure that fills the entire domain. These are often referred to as *localised states*; the building blocks for such solutions can be considered to be isolated regions in which a front exists between a number of periods of the underlying pattern and a homogeneous background state, as illustrated in Figure 1.

Localised states form near subcritical Turing instabilities, in which case two features of the system combine to result in the existence of stable localised states. Firstly, the system is *bistable*, meaning that both the homogeneous and patterned states are linearly stable over an open interval of parameter values. Secondly, a *pinning* mechanism exists so that the configuration of fronts between pattern and homogeneous states is stable.

Physical pattern-forming systems are most commonly modelled through systems of parabolic partial differential equations that describe local interactions: the time evolution of the fields at a point x in the domain depends only on the values of the variables and their derivatives at x itself. However, there are a number of situations in which models containing nonlocal terms emerge as natural descriptions of the dynamics; for example Firth et al. [15] propose a nonlocal model for a nonlinear optical system, Purwins et al. [23] present a nonlocal model for dielectric gas discharge dynamics, and Plaut and Busse [22] derive a nonlocal Complex Ginzburg–Landau equation for the dynamics of thermal convection in a rotating annulus, in a particular parameter regime of low Prandtl numbers. The substantial mathematical biology literature on neural field models contains many examples of nonlocal model equations [17, 28]. The paper by Coombes, Lord and Owen [8] includes numerical evidence for homoclinic snaking in a nonlocal neural field model, although the nonlocality is of a different kind to that considered in this paper.

In this paper we extend the well-known multiple scales asymptotic treatment of the standard 1D Swift–Hohenberg equation

$$\partial_t u = \left[r - (1+\partial_x^2)^2\right] u + N(u), \tag{1.1}$$

for a scalar variable $u(x,t)$, where $N(u)$ denotes nonlinear terms in u and r is a real parameter, to cases where the right-hand side of (1.1) is augmented by a nonlinear nonlocal term of the form $u(K*u^2)$, i.e. $u(x,t)$ multiplied by a convolution of u^2 with a kernel $K(x)$. Such a form includes the example discussed by Firth et al. [15]. Importantly, this choice of nonlocal term also maintains the variational structure of the problem. The variational nature of the standard Swift–Hohenberg equation has been exploited in much recent work since the variational character guarantees, for example, that there are no oscillatory instabilities. For similar reasons of simplification we choose to work with a variational nonlocal term. It is then apparent that (as we show in section 3), proposing a nonlocal term in the free energy function that depends only on u^2, so that the sign of u is immaterial, and which preserves the linear part of the Swift–Hohenberg equation, we are led to the (still rather general) form that we consider here.

We find that consideration of even the 'weakly nonlocal' case, for which the kernel of the nonlocal integral term decays extremely rapidly in space, introduces considerable complexity to the multiple scales analysis. Further complexity arises in the bifurcation structure of the localised states as the width of the kernel increases.

Given the level of complexity we uncover, it is clear that many aspects of this problem deserve a fuller treatment than we are able to give here. In particular, details of the snaking bifurcation structure are left to be the subject of future work. In this paper our focus is on the extension of the multiple scales analysis and the existence of three asymptotic regimes for amplitude equations to operate in.

The paper is organised as follows. In section 2 we summarise briefly the relevant aspects of the behaviour of the local Swift–Hohenberg equation and the formation of localised states. Section 3 introduces the nonlocal term into the Swift–Hohenberg model and makes general remarks on the modified equation. Sections 4 and 5 present the main results of the paper: these extend the standard asymptotic analyses to the weakly nonlocal case in which the kernel function decays on the lengthscale that is asymptotically short in the multiple-scales setup. In section 6 we briefly comment on the two other natural distinguished asymptotic limits of the problem, in which the characteristic lengthscale of the kernel is considered to be longer: these result in the derivation of different Ginzburg–Landau-like equations. Section 7 concludes.

2 Localised states in the 1D Swift–Hohenberg equation

The standard Swift–Hohenberg equation (SHE) given in (1.1) is a one dimensional PDE for the scalar field $u\,(x,t)$ posed on the domain $x \in \Omega \subseteq \mathbb{R}$. It has often been viewed as a near-threshold approximation for Rayleigh-Bénard convection, although it is frequently used in its own right as a canonical model equation for pattern formation, and most recently, as a canonical example of a scalar PDE that has localised solutions and homoclinic snaking [3]. Given suitable nonlinear terms $N(u)$, the base state $u\,(x,t) \equiv 0$ undergoes a pattern-forming instability as r passes through zero. Typically, the nonlinear term incorporates a second parameter whose value determines the criticality of the bifurcation at $r = 0$. In the remainder of this section we review the typical choices of $N(u)$ and the three types of solution to (1.1) prior to discussing the nonlocal form.

The two commonly used variants of the SHE are known as the quadratic-cubic and cubic-quintic cases due to the nonlinear terms they include. We label the two corresponding choices of $N(u)$ by

$$N_{23}(u) = bu^2 - u^3, \qquad \text{and} \qquad N_{35}(u) = su^3 - u^5. \tag{2.1}$$

The N_{35} version is a less generic choice because it is symmetric under sign changes in u. However, the presence of this symmetry makes sense in some physical situations, for example thermal convection in a Boussinesq fluid with identical upper and lower boundary conditions. Certainly, algebraic computations are often much more straightforward with N_{35} compared to N_{23}. In both the N_{23} and N_{35} cases, the term with the smaller exponent controls the extent to which the system exhibits subcritical behaviour at small amplitude, while the term with the larger exponent re-stabilises solutions at large amplitude.

Analysis shows that for $b^2 > \frac{27}{38}$, and for $s > 0$, the Turing instability at $r = 0$ is subcritical; if the reverse inequalities hold then it is supercritical. Both choices of $N(u)$ lead to an equation that is invariant under the spatial reflection $(x,u) \to (-x,u)$. Moreover, changing the sign of b in the N_{23} equation is equivalent to changing the sign of $u(x,t)$. We therefore consider only the cases $b > 0$ and $s > 0$ in what follows.

The solution $u(x,t) \equiv 0$ is linearly stable in $r < 0$ and undergoes a pattern-forming instability at $r = 0$ from which emerges a branch of stationary spatially-periodic solutions. For small r these solutions have wavenumber k close to unity. Other spatially constant branches bifurcate from $u = 0$

at $r = 1$; since these branches lie well away from the initial instability at $r = 0$ their behaviour will not be considered further.

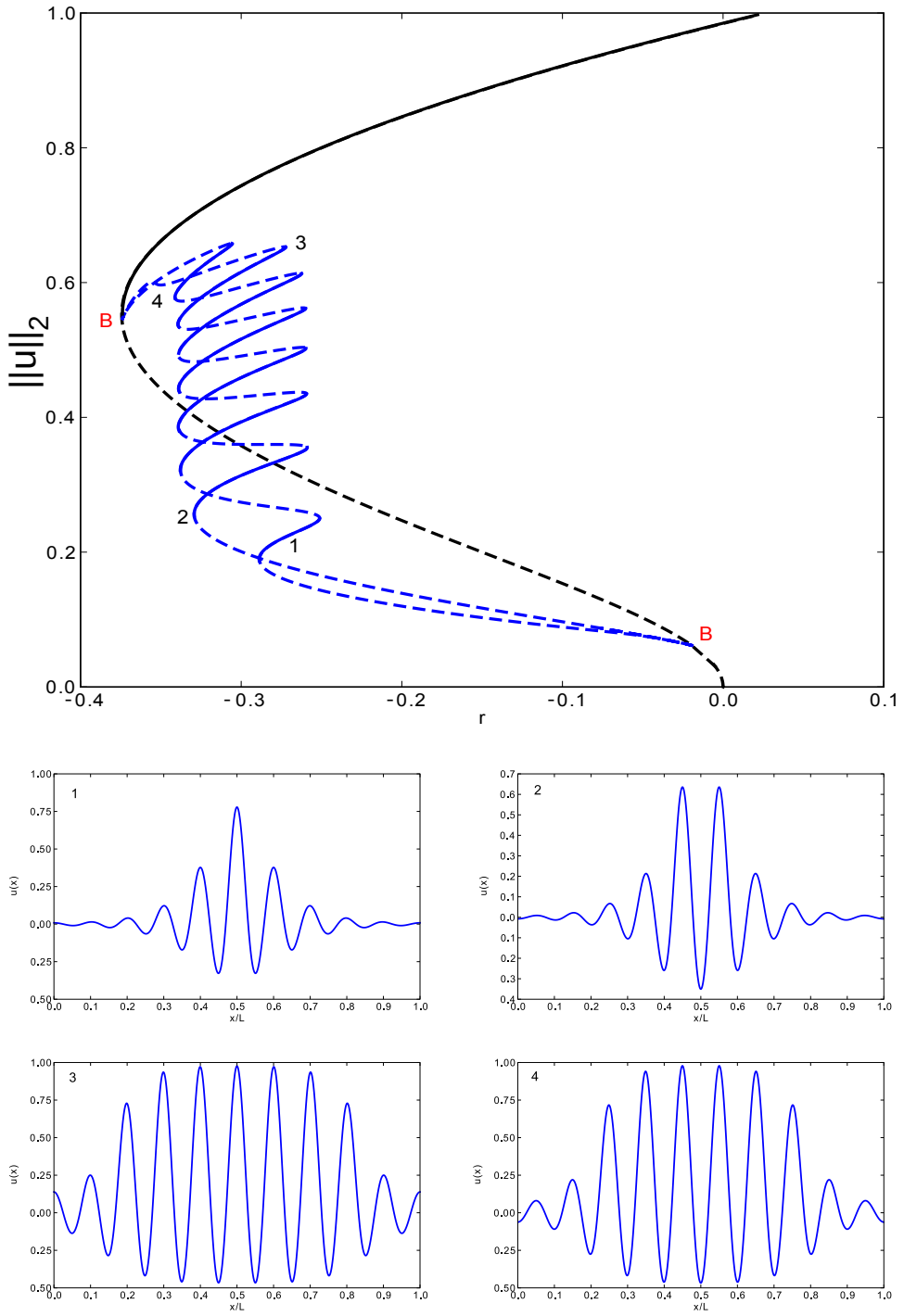

Figure 1: Homoclinic snaking for the SHE. Upper panel: bifurcation diagram showing branches of periodic patterns (black) and localised states (blue) in the $(r, ||u||_2)$-plane for the N_{23} SHE, for $b = 1.8$. Solid (dashed) lines indicate stable (unstable) solutions. Points marked 'B' are the bifurcations at which the localised states emerge from the periodic states and are a consequence of the finite computational domain. Lower panels: illustrative solution profiles $u(x, t)$ at the four numbered locations on the bifurcation diagram. The domain length used is $0 \leq x \leq 20\pi$, with periodic boundary conditions. This figure, and several others, was computed using the continuation software AUTO [14].

When the initial bifurcation at $r = 0$ is subcritical, the patterned branch undergoes a saddle-node bifurcation at finite amplitude in $r < 0$ in both versions of the SHE, illustrated for the N_{23} case in figure 1. In a finite domain, additional bifurcation points (labelled 'B' in the figure) arise along

the branch. In a finite domain these bifurcation points are connected by intertwining branches of modulated solutions that become increasingly localised as the domain size increases. The formation of these intertwining curves is therefore often referred to as 'homoclinic snaking', an (at first sight) unusual structure that has a rich theoretical background as discussed by many authors [6, 9, 4]. Figure 1 also shows typical solution profiles at the top and bottom of each snaking curve. The snaking curves characterise the set of stationary solutions where $u(x)$ describes an orbit that is spatially homoclinic to the state $u(x) \equiv 0$ after exactly one excursion near the periodic pattern. The oscillations in each smooth curve are connected through a set of saddle-node bifurcations that 'snake' backwards and forwards between limiting values of r. For the parameter values of figure 1 this is approximately the interval $-0.34 < r < -0.26$.

Within this snaking region lies a Maxwell point at which the periodic state is energetically equal to the background state, and therefore one would expect stationary fronts between them to be possible. Such a Maxwell point can only be defined for systems that are variational in structure. This is the case for the SHE, and the corresponding free energy quantity is

$$\mathcal{F}[u] = \int_\Omega \left(\frac{1}{2} u_{xx}^2 - u_x^2 + \frac{1-r}{2} u^2 - \int^u N(s)\, ds \right) dx,$$

so that $u_t = -\delta\mathcal{F}/\delta u$ and so

$$\frac{d\mathcal{F}}{dt} = \frac{\partial u}{\partial t}\frac{\delta \mathcal{F}}{\delta u} = -\left(u_t\right)^2 \leq 0,$$

which guarantees convergence to equilibrium states, as long as $\mathcal{F}[u]$ is bounded from below. As one moves up the snake, each additional crossing back-and-forth on the bifurcation diagram is associated with the creation of an additional pair of large amplitude peaks, one at each edge of the localised pattern; solutions at the top of the snake are wider than those at the bottom and the number of turns on the snake is proportional to the size of the domain. In addition to the curves shown in figure 1 there are stationary asymmetric states that exist on 'rungs' that link the two intertwining curves together. The rungs emerge in pitchfork bifurcations near to the saddle-node bifurcation points on the snaking curves. The rung states closely resemble the symmetric localised states on the snaking curves but they have a different phase relation between the small-scale periodic spatial oscillations and their overall envelope. For the SHE they are always unstable. The detailed description of the snaking curves and rung branches demands a close examination of the role of the relative phase between the small-scale and the envelope and this can only be done, in an asymptotic approach, by considering terms that are formally exponentially small. The form of these exponentially small terms has been studied using both exponential asymptotics [19, 7, 13] and the variational approximation method [24, 21, 12].

2.1 Multiple scales asymptotics for the SHE

In this section we review the results of the well-known multiple scales computations for the N_{23} and N_{35} cases of the SHE. To make progress we consider a perturbation expansion that considers small amplitude solutions, introducing the parameter ε to describe the solution amplitude:

$$u(x,t) = \varepsilon u_1 + \varepsilon^2 u_2 + \varepsilon^3 u_3 + \varepsilon^4 u_4 + \varepsilon^5 u_5 + \cdots . \tag{2.2}$$

In addition, the scalar field $u(x,t)$ is modelled as evolving on two different length scales near the bifurcation at $r = 0$: $u(x,t)$ comprises a periodic function on the short lengthscale x, modulated by an unknown envelope $A(X)$ that is a function of a long lengthscale X. In general one would also assume that the two components evolve on different timescales: the underlying pattern varying on the short timescale t, and the envelope evolving on a long timescale T. Since the instability at $r = 0$ is steady, the dependence on t is in fact trivial. We therefore look for leading-order solutions in the form

$$u_1(x, X, t, T) = A(X,T)\, \mathrm{e}^{ix} + \bar{A}(X,T)\, \mathrm{e}^{-ix}, \tag{2.3}$$

where we add the complex conjugate so that u_1 is real even though $A(X,T)$ may be complex-valued. Our last requirement is that the bifurcation parameter r is small which in turn demands that r is rescaled: the rescaled parameter is denoted μ.

We will consider two different sets of parameter scalings. For the SHE the results of the multiple scales calculations are well-known and we give only the results. These provide useful comparisons with the results for the nonlocal SHE presented in section 3. The first set of scalings leads to a solvability condition being imposed at $O(\varepsilon^3)$ in the multiple scales expansion, and results in an

envelope equation that can be solved analytically using Jacobi elliptic functions. The second set of scalings does not require a solvability condition being imposed before $O(\varepsilon^5)$. Although this analysis generates a PDE that does not, in general, have closed form equilibrium solutions, it does provide a leading order estimate of the location of the snaking curves in the bifurcation diagram.

2.2 Derivation of a Ginzburg–Landau equation at third order

The first set of scalings considered is:

$$X = \varepsilon x; \qquad T = \varepsilon^2 t; \qquad r = \varepsilon^2 \mu. \tag{2.4}$$

Proceeding with the standard multiple scales technique of substituting (2.2) into (1.1) and solving for $u_n(x, X, t, T)$ at successive orders in ε we derive evolution equations for $A(X, T)$, in both the N_{23} and N_{35} cases, through the solvability conditions that arise at $O(\varepsilon^3)$. For the N_{23} case we obtain

$$A_T = \mu A + \frac{38}{9}\left(b^2 - \frac{27}{38}\right) A\,|A|^2 + 4A_{XX}, \tag{2.5}$$

and for the N_{35} case we obtain

$$A_T = \mu A + 3sA\,|A|^2 + 4A_{XX}. \tag{2.6}$$

The behaviour and solutions of these cubic Ginzburg–Landau equations are discussed in many places, for example [27] and [16]. The cubic GL equations have explicit solutions in terms of Jacobi elliptic functions. Of more interest for our purposes is that the coefficient of the nonlinear term vanishes in the cases $b^2 = \frac{27}{38}$ and $s = 0$; at these parameter values the pattern-forming instability switches between supercritical and subcritical. Examination of the codimension-two points $(r, b) = (0, \sqrt{27/38})$ and $(r, s) = (0, 0)$ allows us to extend the multiple scales analysis to include the restabilisation of periodic patterns at larger amplitudes; this is considered in the next section.

2.3 Derivation of a Ginzburg–Landau Equation at fifth order

To examine the codimension-two points at which the instability at $r = 0$ switches from supercritical to subcritical we rescale the coefficient of the nonlinear term with the lower exponent, writing

$$b = \sqrt{\frac{27}{38}} + \varepsilon^2 b_2; \qquad \text{or} \qquad s = \varepsilon^2 s_2, \tag{2.7}$$

in the N_{23} and N_{35} cases, respectively. To balance the linear terms in (2.5) and (2.6) at a higher order in the expansion, we introduce the alternative set of scalings

$$X = \varepsilon^2 x; \qquad T = \varepsilon^4 t; \qquad r = \varepsilon^4 \mu. \tag{2.8}$$

No secular terms are generated before $O\left(\varepsilon^5\right)$. At $O(\varepsilon^5)$ we obtain cubic-quintic Ginzburg–Landau equations as follows. For the N_{23} case we obtain

$$A_T = \mu A + \frac{2}{3}\sqrt{114} b_2 A\,|A|^2 - \frac{8820}{361} A\,|A|^4 + i\frac{16}{19} A_X\,|A|^2 + 4A_{XX}, \tag{2.9}$$

and for the N_{35} case we obtain

$$A_T = \mu A + 3s_2 A\,|A|^2 - 10A\,|A|^4 + 4A_{XX}. \tag{2.10}$$

The linear terms are identical to those in (2.5) and (2.6), but the different scalings bring additional nonlinear terms into the asymptotic balance.

The cubic-quintic Ginzburg–Landau equations (2.9) and (2.10) derived at $O(\varepsilon^5)$ are able to capture the bistability through their more complicated collection of competing nonlinear terms. This is illustrated in figure 2.

Figure 2 is clearly similar in structure to figure 1 in that a modulated branch (blue) bifurcates from the primary solution branch (black) at two points, one close to $\mu = 0$ and one close to the saddle node bifurcation. The vertical section of the modulated branch indicates the Maxwell point at which the envelope increases rapidly over a very small range of μ. We note that the cubic-quintic Ginzburg–Landau equation (2.9) and its more general counterparts have been recently investigated by Kao and Knobloch [18] in some detail.

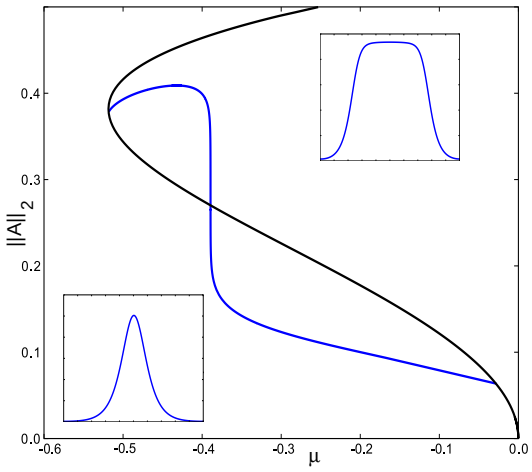

Figure 2: Bifurcation diagram in the $(\mu, \|A\|_2)$ plane for the cubic-quintic Ginzburg–Landau equation (2.9) for $b_2 = 1$ showing the homogeneous (black) and modulated (blue) branches of solutions. The inset figures indicate the general shape of the modulus of the amplitude $|A(X)|$ at two points low down ($\mu \approx -0.1$) and higher up ($\mu \approx -0.4$) on the blue curve. The domain used is $0 \le X \le 20\pi$, with periodic boundary conditions.

3 Including a nonlocal term

Having summarised the usual asymptotic analysis of the local SHE, we now extend it to the case in which an additional nonlinear nonlocal term exists. Specifically we consider the nonlocal Swift–Hohenberg equation

$$\partial_t u = \left[r - (1+\partial_x^2)^2\right] u + N(u) - \gamma u(x,t) \int_\Omega K\left(x-y\right) u\left(y,t\right)^2 \, dy, \tag{3.1}$$

where $K(x)$ is a bounded function defined on Ω that either has bounded support, or decays sufficiently rapidly at large $|x|$, so that its Fourier transform exists. These properties define what we mean by 'short range': we treat the form of $K(x)$ and any parameters on which it depends as fixed while working asymptotically in the limit $\varepsilon \ll 1$.

3.1 Properties of $K(x)$ and the free energy $\mathcal{F}[u]$

We assume also that (i) K is normalised so that $\int_\Omega K(x)\ dx = 1$; (ii) K is even: $K(x) = K(-x) \quad \forall x \in \Omega$, and (iii) K is non-negative: $K(x) \ge 0 \quad \forall x \in \Omega$. The parameter γ is the coefficient of the nonlocal term. The form of the nonlinear nonlocal term proposed in (3.1) is motivated naturally from consideration of the free energy functional

$$\mathcal{F}[u] = \int_\Omega \left(\frac{1}{2} u_{xx}^2 - u_x^2 + \frac{1-r}{2} u^2 - \int^u N(v)\ dv \right) dx + \frac{\gamma}{4} \int_\Omega \int_\Omega K(x-y) u(x)^2 u(y)^2 \, dx\ dy.$$

In order to check that the time evolution $u_t = -\delta\mathcal{F}/\delta u$ is well-posed, we need to ensure that $\mathcal{F}$ is bounded below. In the cubic-quintic case $N(u) = su^3 - u^5$ this is true for all real values of γ. In the quadratic-cubic case $N(u) = bu^2 - u^3$ we require $\gamma > -1$ for $\mathcal{F}$ to be bounded below. These conclusions follow from the following estimate on the size of the nonlocal term in $\mathcal{F}$, deduced by combining the Cauchy–Schwarz inequality and Young's inequality for convolutions. Details of these inequalities can be found, for example, in the textbook by Lieb and Loss [20]. Since the nonlocal term is non-negative we have

$$\begin{aligned} \int_\Omega \int_\Omega K(x-y) u(x)^2 u(y)^2 \, dx\ dy &\equiv \|(K * u^2) u^2\|_1 \\ &\le \|K * u^2\|_2 \ \|u^2\|_2 \\ &\le \|K\|_1 \ \|u^2\|_2 \ \|u^2\|_2 \\ &\le \int_\Omega u(x)^4 \, dx, \end{aligned} \tag{3.2}$$

where we adopt the usual notation $\|f\|_p := \left(\int_\Omega |f|^p \, dx\right)^{1/p}$ for the p-norm of a function $f(x)$, and we have used Cauchy–Schwarz to derive the second line, Young's inequality for the third line, and

the fact that $\|K\|_1 = 1$ (normalisation) for the fourth line. As a result we can see that in $\mathcal{F}[u]$ in the cubic-quintic case the nonlocal term is always dominated by the $\frac{1}{6}u^6$ term in $\mathcal{F}[u]$. In the quadratic-cubic case with $\gamma > 0$ we see that the nonlocal term makes a non-negative contribution to $\mathcal{F}[u]$. In the remaining case, of quadratic-cubic terms with $\gamma < 0$, we can estimate that

$$\mathcal{F}[u] \geq \int_\Omega \frac{1}{2}(u_{xx} + u)^2 - \frac{r}{2}u^2 - \frac{b}{3}u^3 + \frac{1}{4}(1 - |\gamma|)u^4 \, dx$$

which follows after integrating the term $-u_x^2$ by parts and using the estimate (3.2). Hence

$$\mathcal{F}[u] \geq \int_\Omega -\frac{b}{3}u^3 + \frac{1}{4}(1 - |\gamma|)u^4 \, dx,$$

which is bounded below, per unit length of the domain Ω, by $-b^4/(12(1-|\gamma|)^3)$. The bound $\gamma > -1$ is strict since it is attained by the choice of kernel $K(x) = \delta(x)$ the 'Dirac delta' distribution.

3.2 Limiting choices for $K(x)$

There are two limiting choices of $K(x)$ for which the behaviour of solutions to (3.1) can be determined by inspection. The first is the case where $K(x) \equiv \frac{1}{|\Omega|}$, referred to as 'global coupling' in [15]. In this case the bifurcation parameter r is effectively replaced by the new parameter $r' = r - \gamma \langle u^2 \rangle$ where the angled brackets indicate the domain-averaged integral: $\langle u^2 \rangle := \frac{1}{|\Omega|}\int_\Omega u(x,t)^2 dx \equiv \frac{1}{|\Omega|}\|u\|_2^2$. As noted in [15], in this case there is a correspondence between solutions u_{local} and $u_{nonlocal}$ of the local and nonlocal problems, respectively, given by changing the parameter value:

$$u_{nonlocal}\left(x, t; r', \gamma\right) = u_{local}\left(x, t; r - \gamma\left\langle u^2\right\rangle\right). \tag{3.3}$$

The second limiting case is where $K(x) = \delta(x)$, a 'Dirac delta' function. This case amounts to only a change in the nonlinearity from $N(u)$ to $N(u) + \gamma u^3$, i.e. in the N_{23} and N_{35} cases the coefficient of the cubic term is increased by γ.

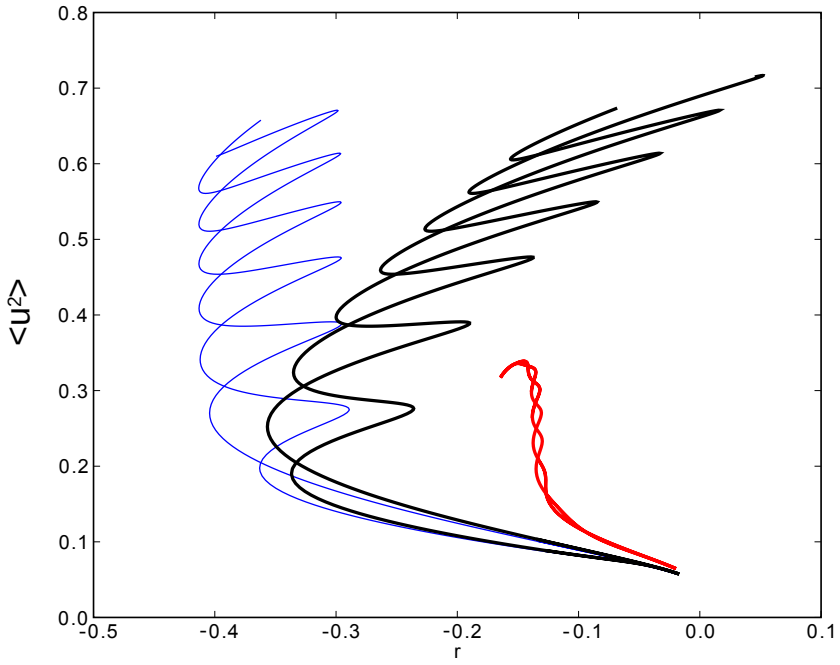

Figure 3: Homoclinic snaking in local and global cases of the (2–3) Swift–Hohenberg equation (3.1). Homoclinic snaking curves in the $(r, \|u\|_2)$ plane are shown for the local case (blue, thin line), and for the nonlocal case (3.1) in the limiting cases $K(x) = \delta(x)$ (red, right-hand curves), and $K = \frac{1}{L}$ (black, sloping curves). Parameter values are $\gamma = 0.7$, $b = 1$. A domain size $L = 20\pi$ and periodic boundary conditions were used. Stability is not indicated.

Figure 3 illustrates the snaking curves for the N_{23} case, for fixed values of the parameters b and γ, varying the choice of kernel function. It confirms the observations made in the paragraph

above: the global coupling case results in a slanted version of the snake from the local problem: they can be mapped onto each other via the relation (3.3). The choice of the Dirac delta function for the kernel produces the smaller snake at r closer to zero: it is vertical rather than slanted since effectively only the coefficient of u^3 has been altered. Since for a general kernel $K(x)$, the nonlocal problem cannot be related directly to a simple transformation of the local problem, and detailed analysis is necessary, the remainder of this paper can be thought of as understanding how the snake shifts between these two limiting cases.

3.3 Homoclinic snaking in the nonlocal SHE

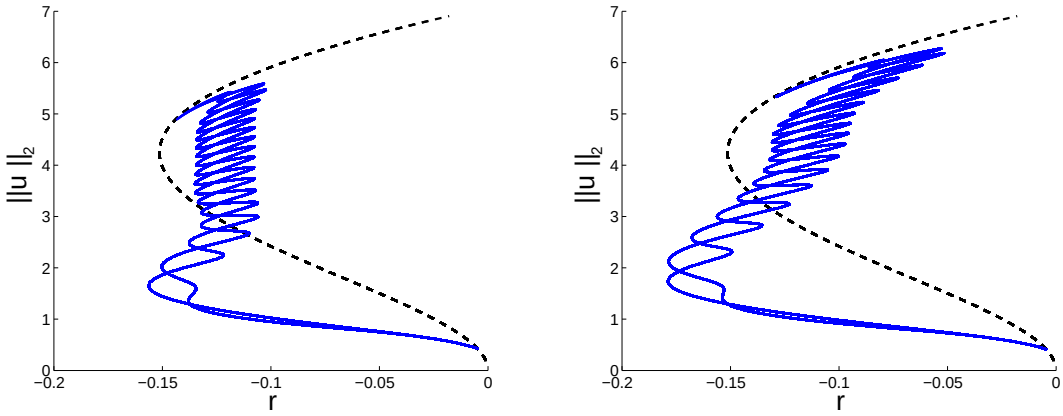

Figure 4: Homoclinic snaking in the nonlocal N_{23} Swift–Hohenberg equation (3.1) with the Gaussian kernel $K_G(x)$ defined in (3.4). Homoclinic snaking curves on which the localised states lie are shown as solid blue lines. Dashed black lines indicate the location of spatially periodic solutions. (a) $\sigma = 4\pi$; (b) $\sigma = 10\pi$. Other parameter values are $\gamma = 0.5$, $b = 1.6$, domain size $L = 40\pi$. Periodic boundary conditions were used, and stability is not indicated.

When the kernel $K(x)$ is assumed either to decay very rapidly, or to decay very slowly compared to the (finite) size of the domain Ω, we might propose that the effect of the nonlocal term is only to shift the snaking curves in r a little from the purely local or purely global problem, respectively. Figure 4 presents bifurcation diagrams for the snaking curves in each of these cases, using the Gaussian kernel

$$K_G(x) = \frac{1}{\sqrt{2\pi\sigma^2}} \mathrm{e}^{-x^2/(2\sigma^2)}. \tag{3.4}$$

In figure 4(a) the width of the Gaussian kernel is $\sigma = 4\pi$ which is small compared to the domain size $L = 40\pi$. The first few turns on the snake are shifted to lower r and the last few slightly shifted to higher r, while the centre of the snake remains close to vertical. Figure 4(b) contains the corresponding snaking bifurcation diagram for $\sigma = 10\pi$ in the same size domain $L = 40\pi$. The homoclinic snaking is stretched out in a manner similar to slanted snaking, but with an overall 'S' shape that the purely global term cannot generate.

It is surprising that the transition between figure 4(a) and figure 4(b) as the width parameter σ increases does not occur in the obvious fashion that one might expect, with the snaking curves deforming smoothly from one figure to the other. Instead, it appears to be a complicated process in which the snaking curves collide with other solution branches, consisting of multipulse states, and re-connect before pinching off again as σ increases further. To illustrate this complex process, figures 5 and 6 present some of the details of the initial changes in bifurcation structure as the kernel width increases, in this case for the top hat kernel

$$K_{TH}(x) = \frac{1}{\delta}\left[H\left(x+\frac{\delta}{2}\right) - H\left(x-\frac{\delta}{2}\right)\right], \tag{3.5}$$

where $H(x)$ denotes the Heaviside function: $H(x) = 0$ if $x \leq 0$ and $H(x) = 1$ if $x > 0$. Figure 5(a) shows the lower end of one of the snaking branches at $\delta = 36$; this value of δ should be considered narrow compared to the overall domain width $L = 40\pi$. Figure 5(b) is computed in the same way for the slightly increased value $\delta = 38$. The snaking curve has collided with two isolas, leading

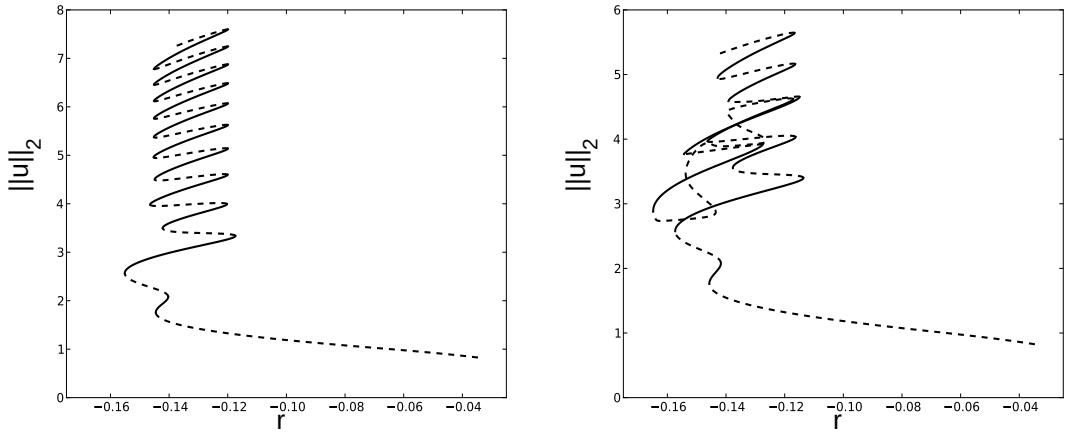

Figure 5: Bifurcation diagrams in the $(r, \|u\|_2)$ plane illustrating homoclinic snaking in the nonlocal N_{23} Swift–Hohenberg equation (3.1) with the top hat kernel $K_{TH}(x)$ defined in (3.5). (a) $\delta = 36$; (b) $\delta = 38$. Other parameter values are $\gamma = 0.5$, $b = 1.6$, domain size $L = 40\pi$. Periodic boundary conditions were used, and solid (dashed) lines indicate stable (unstable) solutions.

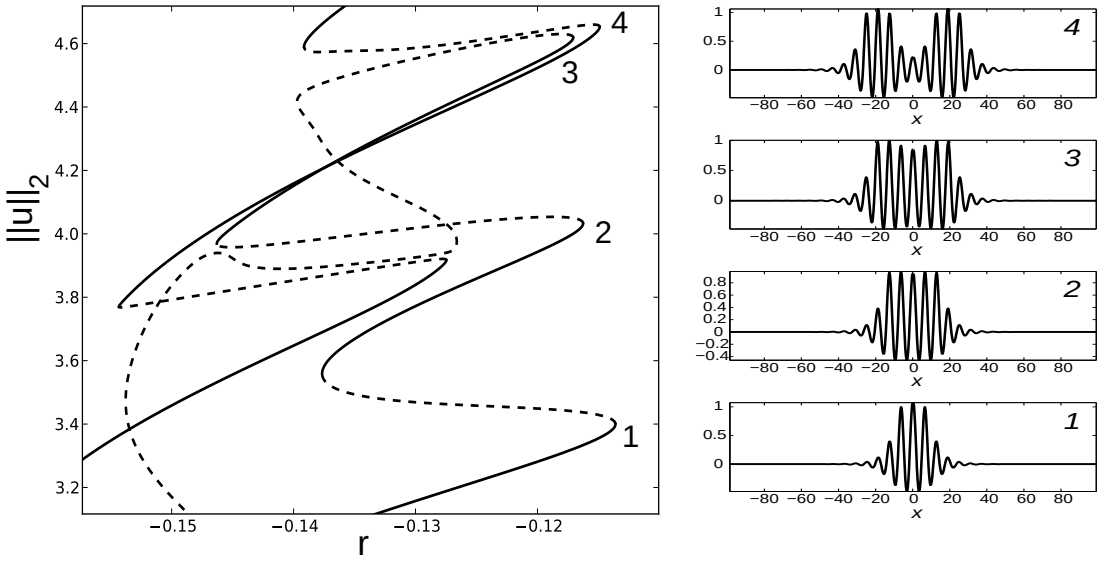

Figure 6: Homoclinic snaking in nonlocal versions of the N_{23} Swift–Hohenberg equation (3.1) with a top hat kernel $K_{TH}(x)$. (a) Enlargement of figure 5(b); (b) solution profiles at the four points labelled 1–4 in (a). Other parameter values are $\gamma = 0.5$, $b = 1.6$, domain size $L = 40\pi$. Periodic boundary conditions were used, and solid (dashed) lines indicate stable (unstable) solutions.

to a number of additional loops over which the solution amplitude, as measured by the L_2 norm, decreases. Such loops were referred to as 'switchbacks' by Taylor & Dawes [25]. Figure 6(a) is an enlargement of part of figure 5(b) that shows the reconnection of several parts of the snaking curve to link to the isolas. Figure 6(b) presents plots of the solution $u(x)$ at the four saddle-node bifurcation points on the right-hand side of figure 6(a), in sequence as the L_2 norm increases. Despite the upper pair occurring very close to each other both in L_2 norm and values of r, the solutions look very different: the upper one is clearly related to a multipulse localised state. Very similar behaviour is observed for the Gaussian kernel; the formation of switchbacks in general appears not to be related to the choice of kernel.

Figures 3 and 4 lay out the challenges that we analyse in detail in the remainder of the paper: developing the well-known multiple-scale analysis to include nonlocal terms allows us to determine the location of the branches of localised states and captures the 'S' shaped nature of the branches as shown in figure 4. As is also well-known, the regular multiple-scales analysis does not shed

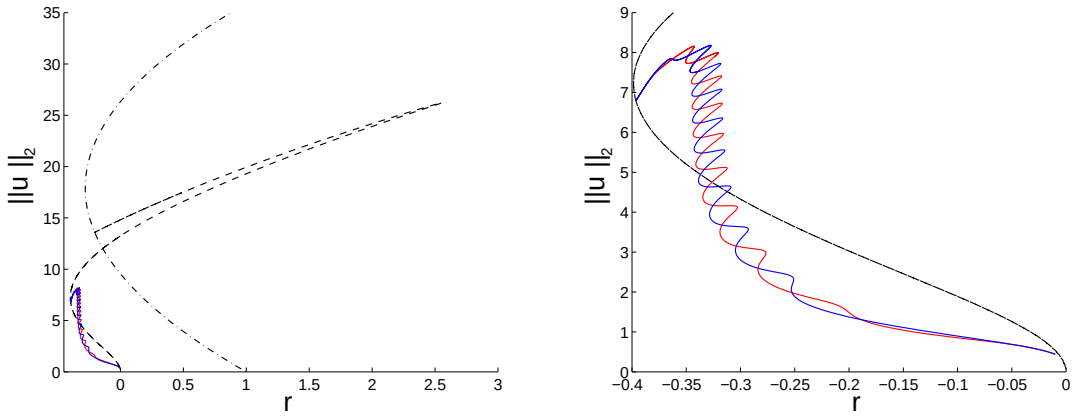

Figure 7: Left: Bifurcation diagram for solutions of the nonlocal Swift–Hohenberg equation (3.1) with a Gaussian kernel, for $\gamma = -0.5$. Dashed line indicates the branch of spatially periodic states that bifurcates from the trivial state at $r = 0$. Dashed-dotted line indicates the non-zero constant state that bifurcates from the trivial state at $r = 1$. Solid (red and blue) curves are the branches of localised states. Stability is not shown. Other parameter values are $\sigma = 4\pi$, $b = 1.6$, domain size $L = 40\pi$.

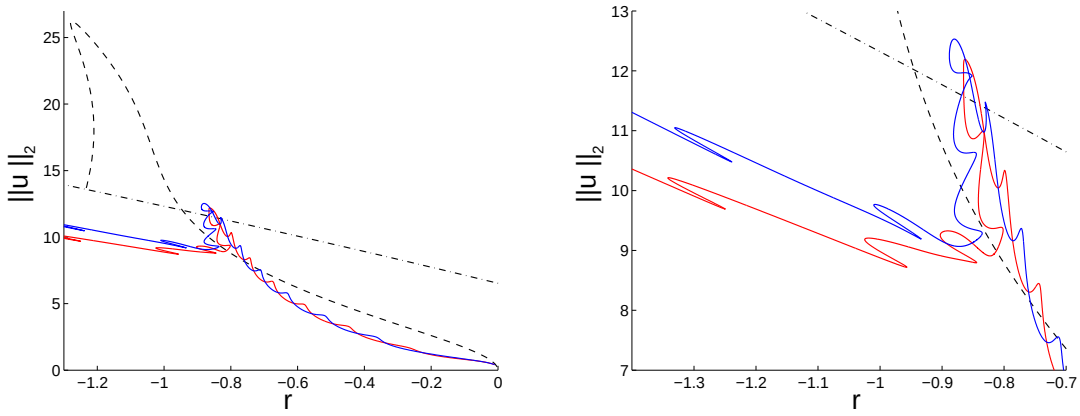

Figure 8: Left: Bifurcation diagram for solutions of the nonlocal Swift–Hohenberg equation (3.1) with a Gaussian kernel, for $\gamma = -1.2$. Dashed line indicates the branch of spatially periodic states that bifurcates from the trivial state at $r = 0$. Dashed-dotted line indicates the non-zero constant state that bifurcates from the trivial state at $r = 1$. Solid (red and blue) curves are the branches of localised states. Stability is not shown. Other parameter values are $\sigma = 4\pi$, $b = 1.6$, domain size $L = 40\pi$.

light on the behaviour of individual snaking curves, and so we are unable to say anything analytic about the breakup of the snaking curves and the collisions with branches of multipulse states that are clearly shown in figures 5 and 6. We suspect that the details of these collisions are strongly dependent on the precise form chosen for the kernel $K(x)$ and we leave these details to be the subject of future work.

Finally, figures 7 and 8 show results for $\gamma = -0.5$ and $\gamma = -1.2$, respectively, using the Gaussian kernel $K_G(x)$ with $\sigma = 4\pi$. The case $\gamma = -0.5$ shows standard homoclinic snaking with branches of localised states reconnecting to the spatially periodic branch near its usual saddle-node bifurcation as the localised state expands to fill the entire domain. One might expect the snaking curves to be tilted backwards, which they are at the lower end but they remain vertical in the central section, as in the case $\gamma = 0.5$ shown in figure 4(a). Figure 7 shows that the branch of spatially periodic states that bifurcates from $r = 0$ (and shown as a dashed line) extends into $r > 0$ before turning round at a second saddle-node point and then terminating on the branch of non-zero spatially constant states (shown as the dash-dotted line) that bifurcates from $r = 1$. This point is therefore another Turing-type instability, this time of the non-zero constant solution.

Numerical investigations reveal that the usual homoclinic snaking structure persists, for $\sigma = 4\pi$, down to around $\gamma = -1.13$ and certainly into $\gamma < -1$. But below a critical value, the localised

states undergo new instabilities in which the central peaks of the localised state widen significantly. These snaking curves do not reconnect to the periodic branch, but instead extend into negative r, undergoing a number of additional twists and turns. This behaviour is illustrated in figure 8. We remark also that taking γ large and negative changes the behaviour of the constant and spatially periodic branches: in figure 8 we observe that the branch of spatially periodic states (dashed line) evolves monotonically until reaching a first saddle-node bifurcation at $r \approx -1.2$, and that the branch of positive constant solutions (dash-dotted line) extends into $r < 0$ and does not undergo a saddle-node bifurcation.

4 Derivation of cubic Ginzburg–Landau equations

In this section we discuss the construction of amplitude equations in the simplest case, in which the kernel $K(x)$ varies only on the short length scale. Equivalently, this is the case where all terms posed on the long length scale X are assumed to be almost constant over the region where the kernel is large. This makes sense in the case that the envelope function is smooth and the kernel function decays much more rapidly than the envelope; hence on functions of X, the kernel $K(x)$ acts to leading order in ε, as a Dirac δ-distribution. This statement will be made more precise in section 5.1 below. For the moment we will illustrate the computations involved in deriving the modifications to the cubic Ginzburg–Landau equations (2.5) and (2.6) when the nonlocal term is included.

Within the weakly nonlinear multiple scales expansion (2.2), we can see by inspection that the presence of the nonlinear nonlocal term contributes only at $O(\varepsilon^3)$ and higher. Direct substitution of the ansatz (2.2) into the nonlocal term indicates that, at the orders in ε that are of interest in deriving the solvability conditions at third or fifth order in ε, the following terms need to be evaluated:

$$O\left(\varepsilon^3\right): \qquad \mathcal{I}_3 := u_1\left(x\right) J_{11}, \tag{4.1}$$

$$O\left(\varepsilon^4\right): \qquad \mathcal{I}_4 := u_2\left(x\right) J_{11} + 2u_1(x) J_{12}, \tag{4.2}$$

$$O\left(\varepsilon^5\right): \qquad \mathcal{I}_5 := u_3\left(x\right) J_{11} + 2u_2\left(x\right) J_{12}, + u_1\left(x\right)\left(2J_{13} + J_{22}\right), \tag{4.3}$$

where the integrals $J_{ij}(x)$ for $i, j \in \{1, 2, 3\}$ are defined to be

$$J_{ij}(x) := \int_\Omega K\left(x - y\right) u_i\left(y\right) u_j\left(y\right)\, dy. \tag{4.4}$$

To simplify the presentation we will carry out the computations initially for two explicit kernel functions: the Gaussian $K_G(x)$ defined in (3.4) and the piecewise-constant top hat function $K_{TH}(x)$ defined in (3.5). Since the scalings (2.4) generate secular terms at $O(\varepsilon^3)$ and higher, for the cubic Ginzburg–Landau equations we need only to evaluate the leading-order part of the expression (4.1) and then incorporate any additional resonant terms (i.e. those having a short-scale dependence $\sim \mathrm{e}^{\pm \mathrm{i}x}$) into the Ginzburg-Landau equations (2.5) and (2.6) derived previously. Substituting the ansatz (2.3) into (4.1) we obtain

$$J_{11} \quad = \quad \int_\Omega K\left(x - y\right)\left(2\left|A(Y)\right|^2 + A(Y)^2 \mathrm{e}^{2\mathrm{i}y} + \bar{A}(Y)^2 \mathrm{e}^{-2\mathrm{i}y}\right) dy.$$

To determine the leading order contribution we consider the envelope $A(Y)$ to be constant within the integral, using the implicit decoupling of the short and long length scales x and $X = \varepsilon x$ that arises asymptotically as $\varepsilon \to 0$. We therefore obtain the leading order simplification

$$\begin{aligned} J_{11} \quad = \quad & 2\left|A(X)\right|^2 \int_\Omega K\left(x - y\right) dy + A(X)^2 \int_\Omega K\left(x - y\right) \mathrm{e}^{2\mathrm{i}y} dy \\ & + \bar{A}(X)^2 \int_\Omega K\left(x - y\right) \mathrm{e}^{-2\mathrm{i}y} dy \; + O(\varepsilon). \end{aligned} \tag{4.5}$$

We now evaluate these contributions in the cases of top hat and Gaussian kernels.

4.1 The top hat kernel $K_{TH}(x)$

In this subsection we evaluate the integrals in (4.5) for the top hat kernel $K_{TH}(x)$ given in (3.5). The computations are the same regardless of the choice of a finite domain Ω or an infinite domain

$\Omega = \mathbb{R}$, assuming that the width δ of the support of $K_{TH}(x)$ is at most the domain length L. Explicitly we obtain

$$J_{11} = \frac{2}{\delta}|A(X)|^2 \int_{x-\frac{\delta}{2}}^{x+\frac{\delta}{2}} dy + \frac{1}{\delta}A(X)^2 \int_{x-\frac{\delta}{2}}^{x+\frac{\delta}{2}} \mathrm{e}^{2iy} dy + \frac{1}{\delta}\bar{A(X)}^2 \int_{x-\frac{\delta}{2}}^{x+\frac{\delta}{2}} \mathrm{e}^{-2iy} dy.$$

Recall the general result, for integer m, that

$$\frac{1}{\delta}\int_{x-\frac{\delta}{2}}^{x+\frac{\delta}{2}} \mathrm{e}^{imy} dy = \mathrm{e}^{imx}\frac{\sin(m\delta/2)}{m\delta/2}, \tag{4.6}$$

which we use in the three cases $m = -2, 0, 2$ to obtain

$$J_{11} = 2|A(X)|^2 + \frac{\sin\delta}{\delta}\left(A(X)^2\mathrm{e}^{2ix} + \bar{A(X)}^2\mathrm{e}^{-2ix}\right).$$

From J_{11} it is straightforward to compute $\mathcal{I}_3$:

$$\mathcal{I}_3 = \left(2 + \frac{\sin\delta}{\delta}\right)A|A|^2\mathrm{e}^{ix} + \left(\frac{\sin\delta}{\delta}\right)A^3\mathrm{e}^{3ix} + c.c.,$$

where *c.c.* denotes the complex conjugate, so that $\mathcal{I}_3$ is always real-valued. Comparison with the calculations in the previous sections shows that in the presence of the nonlocal term with kernel $K_{TH}(x)$ we obtain the Ginzburg–Landau equations

$$A_T = \mu A + \left[\frac{38}{9}\left(b^2 - \frac{27}{38}\right) - \gamma\left(2 + \frac{\sin\delta}{\delta}\right)\right]A|A|^2 + 4A_{XX}, \tag{4.7}$$

for the N_{23} case, and

$$A_T = \mu A + \left[3s - \gamma\left(2 + \frac{\sin\delta}{\delta}\right)\right]A|A|^2 + 4A_{XX}, \tag{4.8}$$

for the N_{35} case. Alternatively, the effect of the nonlocal term can be described as an effective shift in the coefficient of the nonlinear term. In both cases the effect of the nonlocal term is, when $\gamma > 0$, always to make the coefficient of the nonlinear term more negative (since $|\sin\delta| \le \delta$ for all positive δ), and hence the instability is always more supercritical in the presence of the nonlocal term. If $\gamma < 0$ then the nonlocal term makes the instability more subcritical.

4.2 The Gaussian kernel $K_G(x)$

By substituting (3.4) into (4.5) and taking the domain $\Omega := [-L/2, L/2]$, the leading order contribution from J_{11} to the integral term $\mathcal{I}_3$ for the Gaussian kernel $K_G(x)$ on the short length scale only can be expressed as

$$\begin{aligned} J_{11} &= \int_\Omega K(x-y)\left(2|A(Y)|^2 + A(Y)^2\mathrm{e}^{2iy} + \bar{A}(Y)^2\mathrm{e}^{-2iy}\right)dy + O(\varepsilon) \\ &= \frac{2}{\sqrt{2\pi\sigma^2}}|A(X)|^2\hat{I}_1 + \frac{1}{\sqrt{2\pi\sigma^2}}A(X)^2\hat{I}_2 + \frac{1}{\sqrt{2\pi\sigma^2}}\bar{A}(X)^2\hat{I}_3 \end{aligned}$$

where

$$\hat{I}_1 = \int_{-\frac{L}{2}}^{\frac{L}{2}} \mathrm{e}^{-\frac{(x-y)^2}{2\sigma^2}}\, dy, \qquad \hat{I}_2 = \int_{-\frac{L}{2}}^{\frac{L}{2}} \mathrm{e}^{-\frac{(x-y)^2}{2\sigma^2}}\mathrm{e}^{2iy}\, dy, \qquad \hat{I}_3 = \int_{-\frac{L}{2}}^{\frac{L}{2}} \mathrm{e}^{-\frac{(x-y)^2}{2\sigma^2}}\mathrm{e}^{-2iy}\, dy. \tag{4.9}$$

These integrals can be evaluated straightforwardly in terms of the (complex-valued) error function, which we define as: $\mathrm{erf}(z) = \frac{2}{\sqrt{\pi}}\int_0^z e^{-t^2}dt$. We obtain

$$\hat{I}_1 = \frac{\sqrt{2\pi\sigma^2}}{2}G_1(x), \qquad \hat{I}_2 = \frac{\sqrt{2\pi\sigma^2}}{2}\mathrm{e}^{-2\sigma^2}\mathrm{e}^{2ix}G_2(x), \qquad \hat{I}_3 = \frac{\sqrt{2\pi\sigma^2}}{2}\mathrm{e}^{-2\sigma^2}\mathrm{e}^{-2ix}\bar{G}_2(x),$$

where

$$G_1(x) := \operatorname{erf}\left(\frac{x+\frac{L}{2}}{\sqrt{2\sigma^2}}\right) - \operatorname{erf}\left(\frac{x-\frac{L}{2}}{\sqrt{2\sigma^2}}\right),$$
$$G_2(x) := \operatorname{erf}\left(\frac{x+\frac{L}{2}+2i\sigma^2}{\sqrt{2\sigma^2}}\right) - \operatorname{erf}\left(\frac{x-\frac{L}{2}+2i\sigma^2}{\sqrt{2\sigma^2}}\right),$$

and in computing $\hat{I}_3$ we have used the property that $\operatorname{erf}(\bar{z}) = \overline{\operatorname{erf}(z)}$ Putting all this together we obtain the leading order approximation

$$J_{11} = |A(X)|^2 G_1(x) + \frac{1}{2}\mathrm{e}^{-2\sigma^2}\left(G_2(x)A(X)^2\mathrm{e}^{2ix} + \bar{G}_2(x)\bar{A}(X)^2\mathrm{e}^{-2ix}\right) + O(\varepsilon).$$

As with the derivation in the previous subsection for the top hat kernel, we now multiply by $u_1(x)$ and collect terms in like powers of of e^{ix} to compute $\mathcal{I}_3$. This gives

$$\mathcal{I}_3 = \left(G_1(x) + \frac{1}{2}\mathrm{e}^{-2\sigma^2}G_2(x)\right)A|A|^2\mathrm{e}^{ix} + \frac{1}{2}\mathrm{e}^{-2\sigma^2}G_2(x)A^3\mathrm{e}^{3ix} + c.c.. \tag{4.10}$$

Extracting the resonant terms for the Ginzburg–Landau equation from (4.10) by multiplying by e^{-ix} and integrating over Ω is substantially more difficult in the case of a finite domain; we therefore consider the case $L \to \infty$ in order to make further progress. In this limit we find that the functions G_1 and G_2 tend to constant values: $G_1 = G_2 = 2$. For the N_{23} and N_{35} cases, respectively, we obtain the following Ginzburg–Landau equations:

$$A_T = \mu A + \left[\frac{38}{9}\left(b^2 - \frac{27}{38}\right) - \gamma\left(2 + e^{-2\sigma^2}\right)\right]A|A|^2 + 4A_{XX}, \tag{4.11}$$
$$A_T = \mu A + \left[3s - \gamma\left(2 + \mathrm{e}^{-2\sigma^2}\right)\right]A|A|^2 + 4A_{XX}. \tag{4.12}$$

As in the top hat case, the effect of the nonlocal term at this order is therefore effectively to shift the coefficient of the nonlinear term. The shifts are in the same directions as in the case of a top hat kernel. If $\gamma > 0$ then the shift makes the bifurcation behaviour more supercritical. In the limit of a narrow kernel, $\sigma \to 0$, we see that the results from the Gaussian case agree with those of the Dirac 'delta function' discussed at the beginning of section 3 which shifts the coefficient of the cubic term in $N(u)$ either from -1 to $-1+\gamma$ (in the N_{23} case) or from s to $s+\gamma$, in the N_{35} case. This agreement is found also in the top hat case, as can be seen by considering the limit $\delta \to 0$ in (4.7) and (4.8).

In the opposite limits, of wide kernels, where $\sigma \to \infty$ in the Gaussian case, and $\delta \to \infty$ in the top hat case, the coefficients again converge to the same values, although the convergence is oscillatory for the top hat kernel and monotonic for the Gaussian case.

5 Derivation of a cubic-quintic Ginzburg–Landau equation

In order to go beyond the solvability condition at $O\left(\varepsilon^3\right)$ we need to incorporate higher-order contributions from the nonlocal term. This is a necessary preliminary to the investigation of the effects of the nonlocal term on the cubic-quintic Ginzburg–Landau equations near the codimension-two point at which the initial instability changes from supercritical to subcritical. In order to organise this calculation clearly, we first present our approach to the nonlocal term, before using these results in dealing order by order with the multiple scales computation.

5.1 Series expansion of the nonlocal term

In this section we develop an asymptotic expansion of the nonlocal term as a series in the envelope $A(X)$ and its derivatives. The first term in this new expansion is the one that we have relied on in previous calculations. It turns out that we are able to derive a compact and general expression in terms of Fourier coefficients of the kernel: our expansion is therefore applicable to any kernel function that has a well defined, continuously differentiable Fourier transform.

The first step is to observe that all the integrals generated by the asymptotic analysis can be written in the general form

$$J = \int_\Omega K(x-y)\,F[A(Y)]\,\mathrm{e}^{imy}\,dy, \tag{5.1}$$

where F is a function of the amplitude $A(X)$. We adopt the rescalings (2.8), i.e. $X = \varepsilon^2 x$, and we consider the domain $\Omega = \mathbb{R}$. We assume throughout that there are no technical difficulties with applying the Fourier transform. We use the following notation for the Fourier transform and its inverse:

$$\mathcal{F}\left[f\left(x\right)\right]\left(k\right) \equiv \hat{f}\left(k\right) \quad := \quad \int_{-\infty}^{\infty} f\left(x\right) \mathrm{e}^{-ikx}\, dx, \tag{5.2}$$

$$\mathcal{F}^{-1}\left[\hat{f}\left(k\right)\right]\left(x\right) \equiv f\left(x\right) \quad := \quad \frac{1}{2\pi}\int_{-\infty}^{\infty} f\left(k\right) \mathrm{e}^{ikx}\, dk. \tag{5.3}$$

We expand J asymptotically in a series of straightforward steps which we now present. First, we make the substitution $Y = \varepsilon^2 y$ in (5.1), and change the integration variable from y to $z = y - x$ to give

$$J = \int_{\mathbb{R}} K\left(x-y\right) F\left[A\left(Y\right)\right] \mathrm{e}^{imy} dy = \int_{\mathbb{R}} K\left(-z\right) F\left[A\left(\varepsilon^2 x + \varepsilon^2 z\right)\right] \mathrm{e}^{im(x+z)}\, dz.$$

Now we Taylor expand $A(Y)$ about the point X, which gives

$$J \quad = \quad \int_{\mathbb{R}} K\left(-z\right) \mathrm{e}^{im(x+z)} \sum_{n=0}^{\infty} \frac{\left(\varepsilon^2 z D_X\right)^n}{n!} F\left[A\left(X\right)\right]\, dz, \tag{5.4}$$

where D_X stands for d/dX. Reversing the change of integration variable yields

$$J \quad = \quad \int_{\mathbb{R}} K\left(x-y\right) \mathrm{e}^{imy} \left[\sum_{n=0}^{\infty} \frac{\left(-\varepsilon^2 D_X\right)^n}{n!} F\left[A\left(X\right)\right] \left(x-y\right)^n\right]\, dy.$$

We now take all the y-independent terms outside the integral to obtain

$$J \quad = \quad \sum_{n=0}^{\infty} \frac{\left(-\varepsilon^2 D_X\right)^n}{n!} F\left[A\left(X\right)\right] \int_{\mathbb{R}} \left(x-y\right)^n K\left(x-y\right) \mathrm{e}^{imy}\, dy. \tag{5.5}$$

The integral part of this expression is a convolution and so can be written (very compactly) in terms of Fourier transforms:

$$\int_{-\infty}^{\infty} \left(x-y\right)^n K\left(x-y\right) \mathrm{e}^{imy} dy \quad = \quad \mathcal{F}^{-1}\left[\mathcal{F}\left[x^n K\left(x\right)\right] \mathcal{F}\left[\mathrm{e}^{imx}\right]\right]. \tag{5.6}$$

This expression can be simplified significantly further using the well-known Fourier transform properties that (i) the Fourier transform of a complex exponential is a Dirac delta function and and (ii) the effect of multiplication by a power of x:

$$\int_{-\infty}^{\infty} \mathrm{e}^{i(m-k)x}\, dx = 2\pi\delta\left(m-k\right), \qquad \text{and} \qquad \int_{-\infty}^{\infty} x^n K\left(x\right) \mathrm{e}^{-ikx}\, dx = \left(iD_k\right)^n \hat{K}\left(k\right). \tag{5.7}$$

On substituting (5.7) into (5.6), we obtain

$$\begin{aligned} \int_{-\infty}^{\infty} \left(x-y\right)^n K\left(x-y\right) \mathrm{e}^{imy} dy \quad &= \quad 2\pi\mathcal{F}^{-1}\left[i^n D_k^n \hat{K}\ \delta\left(m-k\right)\right] \\ &= \quad \int_{-\infty}^{\infty} i^n D_k^n \hat{K}\ \delta\left(m-k\right) \mathrm{e}^{ikx} dk = \mathrm{e}^{imx}\left(iD_k\right)^n\ \hat{K}\left(k\right)\Big|_{k=m} \end{aligned}$$

Returning to (5.5) we see that we have the expansion:

$$J = \int_{\mathbb{R}} K\left(x-y\right) F\left[A\left(Y\right)\right] \mathrm{e}^{imy} dy = \mathrm{e}^{imx} \sum_{n=0}^{\infty} \frac{\left(-i\varepsilon^2 D_X D_k\right)^n}{n!} F\left[A\left(X\right)\right]\ \hat{K}\left(k\right)\Big|_{k=m}. \tag{5.8}$$

For use in the multiple scales analysis, it is convenient to collect the kernel-dependent parts of the expression into a set of coefficients I_{mn} defined by

$$I_{mn} := \left(-iD_k\right)^n\ \hat{K}\left(k\right)\Big|_{k=m}, \tag{5.9}$$

which can then be evaluated at a later point, for a specific choice of kernel. Note that since we consider kernels that are even functions we have the relation $I_{m0} = I_{(-m)0}$. In conclusion we have (formally) derived the series representation

$$\int_{-\infty}^{\infty} K\left(x-y\right) F\left[A\left(Y\right)\right] \mathrm{e}^{imy}\, dy = \mathrm{e}^{imx} \sum_{n=0}^{\infty} I_{mn} \frac{\left(\varepsilon^2 D_X\right)^n}{n!} F\left[A\left(X\right)\right]. \tag{5.10}$$

5.2 Asymptotic expansion

Having found a general expansion for the integrals arising in the multiple scales analysis, it is now possible to carry out the derivation of a cubic-quintic Ginzburg–Landau equation where the nonlocal term is included, using the alternative scalings (2.8) and the expansion (2.2). Previously, under the $O(\varepsilon^3)$ scalings, the nonlocal term was found to introduce a width dependency into the coefficient of the $A|A|^2$ term. Using the more complicated scalings, it is now shown that similar dependencies appear in the higher order $A|A|^4$ term. As stated, we leave the kernel dependent coefficients I_{mn} unevaluated in the derivation and later generate appropriate values for both top hat and Gaussian kernels through equation (5.9).

The procedure for generating the relevant PDE for A through the multiple scales analysis is much the same as that discussed for the local problem in section 2.3. As there are no integral terms at $O(\varepsilon)$ the ansatz for u_1 remains unchanged, as do the scalings for X,T and μ. However, with the addition of the nonlocal term the codimension-two point in the N_{23} equation is no longer $b = \sqrt{\frac{27}{38}}$ and the parameter b must instead be expanded about the point

$$b_0 = \sqrt{\frac{27}{38} + \frac{9\gamma}{38}(2I_{00} + I_{20})}, \tag{5.11}$$

which depends on the form of (the Fourier transform of) the kernel $K(x)$. Explicitly we write

$$b = b_0 + \varepsilon^2 b_2. \tag{5.12}$$

We remark, for reference, that the codimension two point defined by $r = 0$ and $b = b_0$, given by (5.11), corresponds to the codimension-two case of the bifurcation problem in the spatial dynamics setting studied by Woods and Champneys [29]. In that paper the condition $b = b_0$ is the condition $q_2 = 0$ where q_2 is one of the crucial normal form coefficients for determining the qualitative behaviour of solutions near the bifurcation point.

5.3 Detailed derivation of the cubic–quintic amplitude equation

We now present the derivation of the cubic-quintic amplitude equation in detail in order to show exactly how we make (repeated) use of the series expansion (5.10). For clarity, we restate the nonlocal (2–3) Swift–Hohenberg equation (3.1).

$$\partial_t u = \left[r - \left(1 + \partial_x^2\right)^2\right] u + bu^2 - u^3 - \gamma u(x,t) \int_\Omega K(x-y)\, u(y,t)^2 dy.$$

We expand as usual in an asymptotic series:

$$u(x, X, t, T) = \varepsilon u_1 + \varepsilon^2 u_2 + \varepsilon^3 u_3 + \varepsilon^4 u_4 + \varepsilon^5 u_5 + \cdots,$$

and solve order by order in ε until we obtain a non-trivial solvability condition. To simplify notation we define the linear operator

$$\mathcal{L}[u] := -(1 + \partial_x^2)^2 u.$$

Terms at $O(\varepsilon)$ and $O\left(\varepsilon^2\right)$. Since the nonlocal term is cubic in u, it does not affect the forms of u_1 and u_2. Solving at $O(\varepsilon)$ and $O\left(\varepsilon^2\right)$ and using (5.12) we obtain the expected expressions

$$u_1(x, X, t, T) = A(X, T)\, \mathrm{e}^{ix} + \bar{A}(X, T)\, \mathrm{e}^{-ix},$$

and

$$u_2 = b_0 \left(2|A|^2 + \frac{1}{9} A^2 \mathrm{e}^{2ix} + \frac{1}{9} \bar{A}^2 \mathrm{e}^{-2ix}\right). \tag{5.13}$$

Terms at $O(\varepsilon^3)$. $O(\varepsilon^3)$ is the lowest order at which a term from the nonlocal expression enters directly. We have

$$\partial_t u_3 = \mathcal{L}[u_3] - 4\partial_x \partial_X \underbrace{\left(1 + \partial_x^2\right) u_1}_{=0} + 2b_0 u_1 u_2 - u_1^3 - \gamma u_1 \int_\Omega K(x-y)\, u_1^2(y)\, dy, \tag{5.14}$$

and so to find u_3 we need to solve

$$\mathcal{L}[u_3] + 2b_0 u_1 u_2 - u_1^3 - \gamma u_1 \int_\Omega K(x-y)\, u_1^2(y)\, dy = 0.$$

We expand the integral operator by using the series expansion (5.10), noting that all terms in the expansion where $n > 0$ contribute at least an additional factor of ε^2 and hence only the leading order term in J_{11} contributes at this order:

$$\begin{aligned} J_{11} \equiv \int_\Omega K(x-y) u_1^2(y)\, dy &= J_{11}^{(0)} + \varepsilon^2 J_{11}^{(2)} + O(\varepsilon^4) \\ &= 2|A|^2 I_{00} + I_{20}\left(A^2 \mathrm{e}^{2ix} + \bar{A}^2 \mathrm{e}^{-2ix}\right) + O(\varepsilon^2). \end{aligned} \tag{5.15}$$

At this order we ignore $J_{11}^{(2)}$, and, after multiplying by γu_1 we obtain

$$\gamma u_1 \int_\Omega K(x-y)\, u_1^2(y)\, dy = \gamma\left[\mathrm{e}^{ix}(2I_{00} + I_{20}) A|A|^2 + \mathrm{e}^{3ix} I_{20} A^3\right] + c.c. + O(\varepsilon^2) \tag{5.16}$$

The remaining (local) nonlinear terms in (5.14) are

$$\begin{aligned} 2b_0 u_1 u_2 - u_1^3 &= \frac{2}{9} b_0^2 \left(A^3 \mathrm{e}^{3ix} + \bar{A}^3 \mathrm{e}^{-3ix} + 19A|A|^2 \mathrm{e}^{ix} + 19\bar{A}|A|^2 \mathrm{e}^{-ix}\right) \\ &\quad - \left(A^3 \mathrm{e}^{3ix} + 3A|A|^2 \mathrm{e}^{ix} + 3\bar{A}|A|^2 \mathrm{e}^{-ix} + \bar{A}^3 \mathrm{e}^{-3ix}\right) \\ &= \mathrm{e}^{ix}\left(\frac{38}{9} b_0^2 - 3\right) A|A|^2 + \mathrm{e}^{3ix}\left(\frac{2}{9} b_0^2 - 1\right) A^3 + c.c. \end{aligned} \tag{5.17}$$

Combining (5.16) and (5.17) we have

$$\begin{aligned} 2b_0 u_1 u_2 - u_1^3 - \gamma u_1 \int_\Omega K(x-y)\, u_1^2(y)\, dy &= \mathrm{e}^{ix}\left(\frac{38}{9} b_0^2 - 3 - \gamma(2I_{00} + I_{20})\right) A|A|^2 \\ &\quad + \mathrm{e}^{3ix}\left(\frac{2}{9} b_0^2 - 1 - \gamma I_{20}\right) A^3 + c.c.. \end{aligned}$$

The definition (5.11) of b_0 shows that the coefficients of $\mathrm{e}^{\pm ix}$ vanish, and that the coefficient of e^{3ix} can be simplified:

$$\frac{2}{9} b_0^2 - 1 - \gamma I_{20} = \frac{2}{9}\left(\frac{27}{38} + \frac{9\gamma}{38}(2I_{00} + I_{20})\right) - 1 - \gamma I_{20} = -\frac{16}{19} + \frac{2\gamma}{19}(I_{00} - 9I_{20}).$$

We therefore obtain a solution for u_3 in the form

$$u_3 = C_2\left(A^3 \mathrm{e}^{3ix} + \bar{A}^3 \mathrm{e}^{-3ix}\right), \qquad \text{where} \qquad C_2 = -\frac{1}{76} + \frac{\gamma}{608}(I_{00} - 9I_{20}).$$

Terms at $O(\varepsilon^4)$. At fourth order in ε we obtain

$$\begin{aligned} \partial_t u_4 &= \mathcal{L}[u_4] - 4\partial_x \partial_X \left(1 + \partial_x^2\right) u_2 + b_2 u_1^2 + b_0\left(u_2^2 + 2u_1 u_3\right) - 3u_1^2 u_2 \\ &\quad - \gamma u_2 \int_\Omega K(x-y)\, u_1^2(y)\, dy - 2\gamma u_1 \int_\Omega K(x-y)\, u_1(y)\, u_2(y)\, dy \end{aligned} \tag{5.18}$$

which includes contributions from two integral terms: J_{11} and J_{12}. We write this schematically in the form

$$\partial_t u_4 = \mathcal{L}[u_4] + f_{4L} + f_{4NL},$$

collecting the local and integral terms into f_{4L} and f_{4NL} respectively so that we can consider them separately in what follows.

Local terms at $O(\varepsilon^4)$. Expanding the four local terms we obtain:

$$\begin{aligned} -4\partial_x \partial_X \left(1 + \partial_x^2\right) u_2 &= \frac{16i}{3} b_0 \left(A A_X \mathrm{e}^{2ix} - \bar{A}\bar{A}_X \mathrm{e}^{-2ix}\right), \\ b_2 u_1^2 &= b_2\left(2|A|^2 + A^2 \mathrm{e}^{2ix} + \bar{A}^2 \mathrm{e}^{-2ix}\right), \\ b_0\left(u_2^2 + 2u_1 u_3\right) &= \frac{326}{81} b_0^3 |A|^4 + \mathrm{e}^{2ix}\left(\frac{4}{9} b_0^3 + 2b_0 C_2\right) A^2 |A|^2 \\ &\quad + \mathrm{e}^{4ix}\left(\frac{b_0^3}{81} + 2b_0 C_2\right) A^4 + c.c., \\ -3u_1^2 u_2 &= -\frac{38}{3} b_0 |A|^4 - \mathrm{e}^{2ix} \frac{20}{3} b_0 A^2 |A|^2 - \mathrm{e}^{4ix} \frac{1}{3} C_1 A^4 - c.c.. \end{aligned}$$

Collecting together all these terms we obtain

$$\begin{aligned} f_{4L} &= \frac{16i}{3}b_0\left(AA_X\mathrm{e}^{2ix}-\bar{A}\bar{A}_X\mathrm{e}^{-2ix}\right)+2b_3\left|A\right|^2+b_3A^2\mathrm{e}^{2ix} \\ &\quad+\left(\frac{326}{81}b_0^3-\frac{38}{3}b_0\right)\left|A\right|^4+\mathrm{e}^{2ix}\left(\frac{4}{9}b_0^3+2b_0C_2-\frac{60}{9}b_0\right)A^2\left|A\right|^2 \\ &\quad+\mathrm{e}^{4ix}\left(\frac{b_0^3}{81}+2b_0C_2-\frac{b_0}{3}\right)A^4+c.c.\ . \end{aligned}$$

Integral terms at $O(\varepsilon^4)$. We now turn to the nonlocal terms. Using the series expansions, the two integral terms are evaluated to give the following:

$$\begin{aligned} J_{11}\equiv\int_\Omega K\left(x-y\right)u_1^2\left(y\right)dy &= 2\left|A\right|^2I_{00}+I_{20}\left(A^2e^{2ix}+\bar{A}^2e^{-2ix}\right), \\ J_{12}\equiv\int_\Omega K\left(x-y\right)u_1\left(y\right)u_2\left(y\right)dy &= \frac{b_0}{9}\left[19I_{10}(A\left|A\right|^2e^{ix}+\bar{A}\left|A\right|^2e^{-ix}\right) \\ &\quad+I_{30}(A^3e^{3ix}+\bar{A}^3e^{-3ix})\right], \end{aligned}$$

ignoring higher-order contributions in ε. The nonlocal terms can then be evaluated to give

$$\begin{aligned} \gamma u_2\int_\Omega K\left(x-y\right)u_1^2\left(y\right)dy &= \gamma b_0\left[\left(4I_{00}+\frac{2}{9}I_{20}\right)\left|A\right|^4+\mathrm{e}^{2ix}\left(2I_{20}+\frac{2}{9}I_{00}\right)A^2\left|A\right|^2\right. \\ &\quad\left.+\frac{I_{20}}{9}A^4\mathrm{e}^{4ix}\right]+c.c., \end{aligned}$$

and

$$\begin{aligned} 2\gamma u_1\int_\Omega K\left(x-y\right)u_1\left(y\right)u_2\left(y\right)dy &= \frac{2}{9}\gamma b_0\left[38I_{10}\left|A\right|^4+\mathrm{e}^{2ix}\left(19I_{10}+I_{30}\right)A^2\left|A\right|^2\right. \\ &\quad\left.+I_{30}A^4\mathrm{e}^{4ix}\right]+c.c.\ . \end{aligned}$$

These contributions to the right hand side of (5.18) can be collected together to give

$$\begin{aligned} f_{4NL} &= \frac{\gamma b_0}{9}\left[\left(36I_{00}+76I_{10}+2I_{20}\right)\left|A\right|^4+\mathrm{e}^{2ix}\left(2I_{00}+38I_{10}+18I_{20}+2I_{30}\right)A^2\left|A\right|^2\right. \\ &\quad\left.+\mathrm{e}^{4ix}\left(I_{20}+2I_{30}\right)A^4\right]+c.c. \end{aligned}$$

Solution at $O(\varepsilon^4)$. The equation for u_4 therefore reduces to

$$0=\mathcal{L}\left[u_4\right]+2b_3\left|A\right|^2+C_3\left|A\right|^4+\left(i\frac{16}{3}C_1AA_X+b_3A^2+C_4A^2\left|A\right|^2\right)\mathrm{e}^{2ix}+C_5A^4\mathrm{e}^{4ix}+c.c. \tag{5.19}$$

where we have defined the constants C_3, C_4 and C_5 to be

$$\begin{aligned} C_3 &= b_0\left[\frac{326}{81}b_0^2-\frac{38}{3}-2\gamma\left(2I_{00}+\frac{38}{9}I_{10}+\frac{1}{9}I_{20}\right)\right], \\ C_4 &= b_0\left[\frac{4}{9}b_0^2+2C_2-\frac{20}{3}-\frac{2\gamma}{9}\left(I_{00}+19I_{10}+9I_{20}+I_{30}\right)\right], \\ C_5 &= b_0\left[\frac{b_0^2}{81}+2C_2-\frac{1}{3}-\frac{\gamma}{9}\left(I_{20}+2I_{30}\right)\right]. \end{aligned}$$

Equation (5.19) can be solved straightforwardly, since there are no terms in $\mathrm{e}^{\pm ix}$, by acting with $\mathcal{L}^{-1}$. We therefore obtain the solution

$$u_4=2b_3\left|A\right|^2+C_3\left|A\right|^4+\left(i\frac{16}{27}C_1AA_X+\frac{b_3}{9}A^2+\frac{C_4}{9}A^2\left|A\right|^2\right)\mathrm{e}^{2ix}+\frac{C_5}{225}A^4\mathrm{e}^{4ix}+c.c.\ .$$

Terms at $O(\varepsilon^5)$. Continuing to fifth order in ε we pick up contributions from three additional integral terms as well as higher-order contributions from J_{11} - recall that at $O(\varepsilon^3)$ we considered only the leading order part of J_{11}. At $O(\varepsilon^5)$ we seek only to identify the coefficients of the $\mathrm{e}^{\pm ix}$ terms in order to deduce a solvability condition; we do not need to solve completely for u_5. Considering terms at $O(\varepsilon^5)$ in (3.1) we have

$$\begin{aligned}\partial_t u_5 + \partial_T u_1 &= \mathcal{L}[u_5] + \left(\mu + 4\partial_X^2\right) u_1 - 4\partial_x\partial_X\left(1+\partial_x^2\right) u_3 + 2b_2 u_1 u_2 + 2b_0\left(u_2 u_3 + u_1 u_4\right) \\ &\quad -3\left(u_1 u_2^2 + u_1^2 u_3\right) - \gamma u_3 \int_\Omega K(x-y)\, u_1^2(y)\, dy \\ &\quad -2\gamma u_2 \int_\Omega K(x-y)\, u_1(y)\, u_2(y)\, dy \\ &\quad -\gamma u_1 \int_\Omega K(x-y)\left(2u_1(y)\, u_3(y) + u_2^2(y)\right) dy, \qquad (5.20) \\ &= \mathcal{L}[u_5] + f_{5L} + f_{5NL}.\end{aligned}$$

Local terms at $O(\varepsilon^5)$. The local terms in (5.20) contribute the following terms that contain a factor of e^{ix} (we list only those terms, and ignore terms containing factors of e^{iqx} where $q \neq 1$):

$$\begin{aligned}\left(\mu + 4\partial_X^2\right) u_1 &= \left(\mu A + 4A_{XX}\right)\mathrm{e}^{ix} + \cdots, \\ 2b_2 u_1 u_2 &= \frac{38}{9} b_2 b_0 A\,|A|^2\,\mathrm{e}^{ix} + \cdots, \\ 2b_0 u_2 u_3 &= \frac{2}{9} b_0^2 C_2 A\,|A|^4\,\mathrm{e}^{ix} + \cdots, \\ 2b_0 u_1 u_4 &= 2b_0\left[\frac{19}{9} b_2 A\,|A|^2 + \left(C_3 + \frac{C_4}{9}\right) A\,|A|^4 + i\frac{16}{27} b_0\,|A|^2 A_X\right]\mathrm{e}^{ix} + \cdots, \\ -3\left(u_1 u_2^2 + u_1^2 u_3\right) &= -\left(\frac{362}{27} b_0^2 + 3C_2\right) A\,|A|^4\,\mathrm{e}^{ix} + \cdots.\end{aligned}$$

Collecting these terms together we obtain, for the local terms,

$$f_{5L} = \left(\mu A + 4A_{XX} + \frac{76}{9} b_0 b_2 A\,|A|^2 + C_6 A\,|A|^4 + i\frac{32}{27} b_0^2 A_X\,|A|^2\right)\mathrm{e}^{ix} + \cdots,$$

where

$$C_6 = \frac{2}{9}\left(b_0^2 C_2 + b_0 C_4\right) + 2b_0 C_3 - 3C_2 - \frac{362}{27} b_0^2.$$

Nonlocal terms that make leading order contributions at $O(\varepsilon^5)$. We consider the contributions made by each of the nonlocal terms in f_{5NL} in turn. As in the case of the local terms, we give only the terms containing a factor of e^{ix}. For each nonlocal term we first give the leading order contribution of the integral term, followed by the terms containing factors of e^{ix} that contribute to the solvability condition. For the first nonlocal term in (5.20) we have

$$\begin{aligned}\int_\Omega K(x-y)\, u_1^2(y)\, dy &= 2\,|A|^2 I_{00} + I_{20}\left(A^2 e^{2ix} + \bar{A}^2 e^{-2ix}\right) + O(\varepsilon^2), \\ \Rightarrow -\gamma u_3 \int_\Omega K(x-y)\, u_1^2(y)\, dy &= -\gamma C_2 I_{20} A\,|A|^4\,\mathrm{e}^{ix} + \cdots + O(\varepsilon^2).\end{aligned}$$

For the second nonlocal term in (5.20) we obtain

$$\begin{aligned}\int_\Omega K(x-y)\, u_1(y)\, u_2(y)\, dy &= \frac{b_0}{9}\left[19 I_{10} A\,|A|^2\,\mathrm{e}^{ix} + I_{30} A^3 \mathrm{e}^{3ix}\right. \\ &\quad \left. +19 I_{10}\bar{A}\,|A|^2\,\mathrm{e}^{-ix} + I_{30}\bar{A}^3 \mathrm{e}^{-3ix}\right], \\ \Rightarrow -2\gamma u_2 \int_\Omega K(x-y)\, u_1(y)\, u_2(y)\, dy &= -\frac{2}{9}\gamma b_0^2\left(38 I_{10} + \frac{19}{9} I_{10}\right. \\ &\quad \left. +\frac{1}{9} I_{30}\right) A\,|A|^4\,\mathrm{e}^{ix} + \cdots + O(\varepsilon^2).\end{aligned}$$

For the third nonlocal term in (5.20) we obtain

$$\begin{aligned}\int_\Omega K(x-y)\,u_1(y)\,u_3(y)\,dy &= C_2\left[A^4\mathrm{e}^{4ix}I_{40}+A^2|A|^2\mathrm{e}^{2ix}I_{20}\right.\\ &\quad\left.+\bar{A}^4\mathrm{e}^{-4ix}I_{40}+\bar{A}^2|A|^2\mathrm{e}^{-2ix}I_{20}\right],\\ \Rightarrow -2\gamma u_1\int_\Omega K(x-y)\,u_1(y)\,u_3(y)\,dy &= -2\gamma C_2(I_{20})\,A|A|^4\mathrm{e}^{ix}+\cdots+O(\varepsilon^2).\end{aligned}$$

For the fourth nonlocal term in (5.20) we obtain

$$\begin{aligned}\int_\Omega K(x-y)\,u_2^2(y)\,dy &= \frac{326}{81}b_0^2|A|^4I_{00}+\frac{4}{9}b_0^2I_{20}\left(A^2|A|^2\mathrm{e}^{2ix}+\bar{A}^2|A|^2\mathrm{e}^{-2ix}\right)\\ &\quad+\frac{b_0^2}{81}I_{40}\left(A^4\mathrm{e}^{4ix}+\bar{A}^4\mathrm{e}^{-4ix}\right),\\ \Rightarrow -\gamma u_1\int_\Omega K(x-y)\,u_2^2(y)\,dy &= -\gamma b_0^2\left(\frac{326}{81}I_{00}+\frac{4}{9}I_{20}\right)A|A|^4e^{ix}+\cdots+O(\varepsilon^2).\end{aligned}$$

These four integral terms therefore contribute a term of the form

$$f_{5NL}^{(0)}=-\gamma C_7A|A|^4\mathrm{e}^{ix}+\cdots, \tag{5.21}$$

to the right hand side of (5.20), where the coefficient C_7 is defined to be

$$C_7=3C_2I_{20}+\frac{b_0^2}{81}\left(326I_{00}+722I_{10}+36I_{20}+2I_{30}\right).$$

Nonlocal terms that introduce higher order contributions at $O(\varepsilon^5)$. At $O\left(\varepsilon^5\right)$ the second term in the series expansion of J_{11} contributes to the solvability condition, see (5.15). Explicitly, we obtain

$$\begin{aligned}\int_\Omega K(x-y)\,u_1^2(y)\,dy &= 2\int_\Omega K(x-y)|A|^2dy+\int_\Omega K(x-y)\,A^2\mathrm{e}^{2ix}dy\\ &\quad+\int_\Omega K(x-y)\,\bar{A}^2\mathrm{e}^{-2ix}dy,\\ &= J_{11}^{(0)}+2\varepsilon^2\left[\left(A_X\bar{A}+A\bar{A}_X\right)I_{01}+AA_X\mathrm{e}^{2ix}I_{21}+\bar{A}\bar{A}_X\mathrm{e}^{-2ix}I_{(-2)\,1}\right].\end{aligned} \tag{5.22}$$

The terms in e^{ix} from this expression that contribute to the solvability condition are found by multiplying (5.22) by γu_1. This gives

$$\gamma u_1\int_\Omega K(x-y)\,u_1^2(y)\,dy=\gamma u_1J_{11}^{(0)}+\varepsilon^2\gamma\mathrm{e}^{ix}\left[2\left(I_{01}+I_{21}\right)A_X|A|^2+2I_{01}\bar{A}_XA^2\right].$$

We remark that when the kernel $K(x)$ is real, as in all the cases we consider, the coefficients I_{m1} are purely imaginary.

Solvability condition at $O(\varepsilon^5)$. Putting all these contributions together we obtain the following cubic–quintic Ginzburg–Landau equation for $A(X,T)$ from the solvability condition at fifth order in ε:

$$A_T=\mu A+4A_{XX}+\frac{76}{9}b_0b_2A|A|^2+(C_6-\gamma C_7)\,A|A|^4+i\left[C_8A_X|A|^2+C_9\bar{A}_XA^2\right], \tag{5.23}$$

where b_0 is defined in (5.11) and

$$\begin{aligned}
C_2 &= -\frac{1}{76} + \frac{\gamma}{608}\left(I_{00} - 9I_{20}\right), \\
C_3 &= b_0\left[\frac{326}{81}b_0^2 - \frac{38}{3} - 2\gamma\left(2I_{00} + \frac{38}{9}I_{10} + \frac{1}{9}I_{20}\right)\right], \\
C_4 &= b_0\left[\frac{4}{9}b_0^2 + 2C_2 - \frac{20}{3} - \frac{2\gamma}{9}\left(I_{00} + 19I_{10} + 9I_{20} + I_{30}\right)\right], \\
C_5 &= b_0\left[\frac{b_0^2}{81} + 2C_2 - \frac{1}{3} - \frac{\gamma}{9}\left(I_{20} + 2I_{30}\right)\right], \\
C_6 &= \frac{2}{9}\left(b_0^2C_2 + b_0C_4\right) + 2b_0C_3 - 3C_2 - \frac{362}{27}b_0^2, \\
C_7 &= 3C_2I_{20} + \frac{b_0^2}{81}\left(326I_{00} + 722I_{10} + 36I_{20} + 2I_{30}\right), \\
C_8 &= \frac{32}{27}b_0^2 + 2\gamma\mathrm{Im}\left(I_{01} + I_{21}\right), \\
C_9 &= 2\gamma\mathrm{Im}(I_{01}).
\end{aligned}$$

The coefficients $C_2, \ldots, C_9$ are real valued: we introduce Im into C_8 and C_9 (assuming that the kernel is real), in order to make this clear. In the case that the kernel K is even-symmetric, we see that the coefficients I_{m1} will vanish, and so $b_0 = 27/38$, $C_8 = 32b_0^2/27 = 16/17$, and $C_9 = 0$. As we expect, every term that contains a factor of I_{mn} also contains at least one factor of γ: in the case $\gamma = 0$ the well-known solvability condition (2.9) for the (2–3) Swift–Hohenberg equation is recovered.

In the case of a real, even-symmetric kernel $K(x)$, the coefficients in the amplitude equation (5.23) simplify a little to give the form

$$A_T = \mu A + 4A_{XX} + \frac{76}{9}b_0b_2A\left|A\right|^2 + C_{10}A\left|A\right|^4 + iC_8A_X\left|A\right|^2,$$

in which the coefficients, expressed directly in terms of values of the Fourier transform $\hat{K}(k)$ and its derivatives, are

$$\begin{aligned}
b_0 &= \sqrt{\frac{27}{38} + \frac{9\gamma}{38}\left(2\hat{K}\left(0\right) + \hat{K}\left(2\right)\right)}, \\
C_8 &= \frac{32}{27}b_0^2 - 2\gamma\left.\frac{d\hat{K}(k)}{dk}\right|_{k=2}, \\
C_{10} &= -\frac{8820}{361} - \gamma\mathbf{v}^T\mathbf{k} - \gamma^2\mathbf{k}^TM\mathbf{k},
\end{aligned}$$

where

$$\mathbf{v} = \begin{bmatrix} \frac{7998}{361} \\ 19 \\ \frac{2764}{361} \\ \frac{1}{19} \end{bmatrix}, \qquad M = \begin{bmatrix} \frac{67415}{17328} & \frac{19}{3} & \frac{14489}{17328} & \frac{1}{57} \\ \frac{19}{3} & 0 & \frac{19}{6} & 0 \\ \frac{14489}{17328} & \frac{19}{6} & -\frac{1059}{5776} & \frac{1}{114} \\ \frac{1}{57} & 0 & \frac{1}{114} & 0 \end{bmatrix}, \qquad \mathbf{k} = \begin{bmatrix} \hat{K}\left(0\right) \\ \hat{K}\left(1\right) \\ \hat{K}\left(2\right) \\ \hat{K}\left(3\right) \end{bmatrix}.$$

The coefficients in the amplitude equation therefore depend only on five pieces of data concerning $\hat{K}(k)$: the values at $k = 0, 1, 2, 3$ and the derivative $\hat{K}'(2)$.

Figure 9 shows the variation of the coefficients C_8 and C_{10} as functions of the kernel width for both the top hat (blue) and Gaussian (black) cases. As anticipated, in the limit of very small and very large width parameters these are indistinguishable, which is consistent with the asymptotic solution of the $O\left(\varepsilon^3\right)$ nonlocal problem.

A final quantity of interest for the Ginzburg–Landau equation (5.24) is the normal form coefficient q_4 that determines the dynamics near the codimension-two point at which $\mu = q_2 = 0$. For a fuller discussion of the meaning of the coefficient q_4 we refer the reader to the paper by Woods and Champneys [29]; brief discussion is contained also in the paper by Burke & Dawes [5]. It is sufficient here to remark that homoclinic snaking, and the consequent existence of localised states over an open interval in $\mu < 0$ is typical in the case $q_2 < 0$ and $q_4 > 0$, whereas in the case $q_4 < 0$

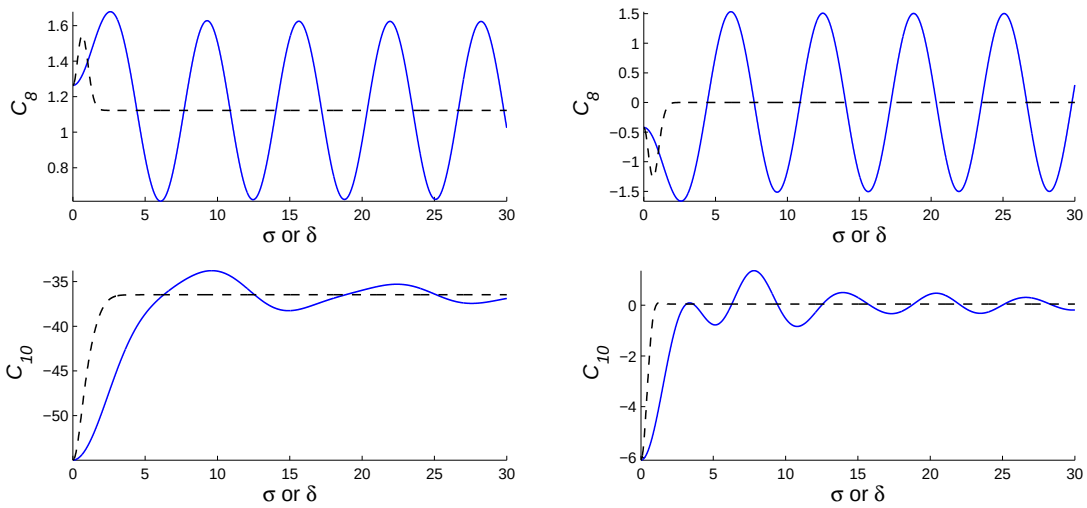

Figure 9: The coefficients C_8 and C_{10} in the fifth order Ginzburg-Landau equation (5.24) plotted as functions of the width parameters δ (for the top hat kernel, solid blue lines) and σ (for the Gaussian kernel, dashed black lines). Left-hand plots are for $\gamma = 0.5$, right-hand plots are for $\gamma = -1.5$. The remaining parameter, b, is determined by the condition $q_2 = 0$, i.e. $b = b_0$ where b_0 is defined in (5.11).

we anticipate the existence of a single localised state, spatially decaying to zero at large $|x|$, that exists for $\mu < 0$ and near zero, for q_2 of either sign. As discussed in [5], q_4 can be computed as a combination of coefficients in the Ginzburg–Landau equation (5.24). For the problem at hand we find

$$q_4 = -\frac{3}{256}C_8^2 - \frac{1}{4}C_{10}. \tag{5.24}$$

This expression for q_4 is relevant in the normal form, strictly speaking, only when $q_2 = 0$; this places an additional constraint on (5.24) so that, for the top hat and Gaussian kernels discussed above, b_0, γ and the kernel width parameter (δ or σ, respectively) are not independent: (5.11) must also be satisfied.

The quadratic dependence of q_4 on γ means that for γ sufficiently large, of either sign, q_4 is positive. Figure 10 illustrates the dependence of q_4 on γ for the top hat and Gaussian kernels, as functions of γ and the width parameters δ and σ. In these plots, for a given point in the parameter plane b_0 is chosen in order to fix $q_2 = 0$. Since both kernels converge weakly to a delta function as the width parameters δ and σ tend to zero, it is perhaps not surprising that the plots agree very closely for small σ and δ.

6 Longer range nonlocal interactions

In the previous section we computed quantitatively how a nonlocal term with a short range kernel shifted the codimension two point $q_2 = 0$ and the location of the snaking curves, by changing the coefficients of the Ginburg–Landau equations that can be derived at $O(\varepsilon^3)$ or $O(\varepsilon^5)$ that provide leading-order descriptions of the weakly nonlinear dynamics. In this section we make brief remarks about the existence of two other distinguished limits in which the width of the kernel can be rescaled so as to enable the derivation of Ginzburg–Landau equations, at $O(\varepsilon^5)$, that capture different details of the effect of the nonlocal term. These distinguished limits also connect the results of the previous section to the slanted snaking since the new terms in the Ginzburg–Landau equations allow the branch of modulated states to deform in novel ways. For simplicity and brevity we present results for the N_{23} Swift–Hohenberg equation and the Gaussian kernel.

In general, in moving away from the narrow kernel limit that we have implicitly worked within so far, we anticipate deriving Ginzburg–Landau equations that contain either higher-order derivatives, or integral terms, in order to capture the nonlocal effects on the long length scale X. Since, as we have commented above, it rapidly becomes difficult to take more than the leading order contribution of the nonlocal term into account, we focus on the leading order term $\gamma u_1 J_{11}$. Using the series

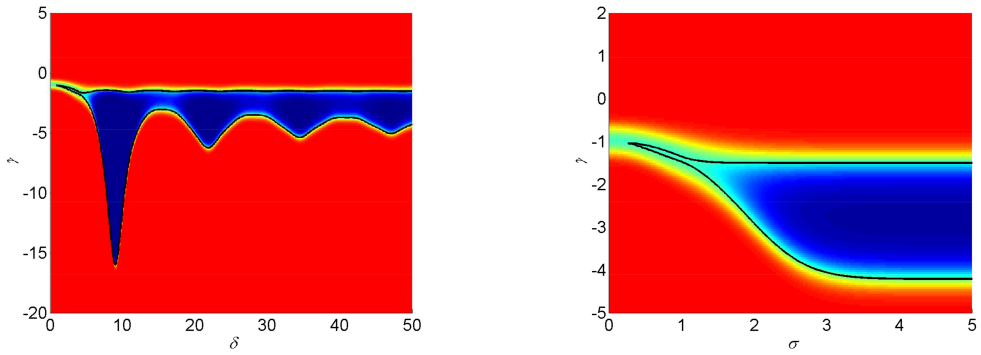

Figure 10: Dependence of q_4 on γ and the kernel width. Light red regions correspond to $q_4 > 0$ and dark blue regions correspond to $q_4 < 0$. The solid black line indicates the set $q_4 = 0$. Left: top hat kernel $K_{TH}(x)$. Right: Gaussian kernel $K_G(x)$.

expansion (5.10) we have the expansion

$$\begin{aligned}\gamma u_1 J_{11} &= -\varepsilon\gamma\left(A\mathrm{e}^{ix} + \bar{A}\mathrm{e}^{-ix}\right)\left[2\sum_{n=0}^{\infty}\frac{\left(\varepsilon^2 D_X\right)^n}{n!}I_{0n}|A|^2(X)\right.\\ &\left.+\mathrm{e}^{2ix}\sum_{n=0}^{\infty}\frac{\left(\varepsilon^2 D_X\right)^n}{n!}I_{2n}A^2(X) + \mathrm{e}^{-2ix}\sum_{n=0}^{\infty}\frac{\left(\varepsilon^2 D_X\right)^n}{n!}I_{(-2)n}\bar{A}^2(X)\right]. \qquad (6.1)\end{aligned}$$

For the Gaussian kernel, for which $\hat{K}(k) = \exp(-\sigma^2 k^2/2)$, table 1 lists the first few coefficients I_{mn} for reference. It is easily seen that in the Gaussian case, the coefficients I_{mn} are closely related to the Hermite polynomials $He_n(x)$. Precisely, we have

$$I_{mn} = (i\sigma)^n\ \mathrm{e}^{-(\sigma m)^2/2}\ He_n(\sigma m),$$

where $He_n(x)$ is the Hermite polynomial of degree n, defined by the expression

$$He_n(x) := \mathrm{e}^{x^2/2}\ (-1)^n\ \left(\frac{d}{dx}\right)^n \mathrm{e}^{-x^2/2},$$

following the notation of Abramowitz & Stegun [1], chapter 22. To look for new distinguished limits we introduce the rescaled kernel width parameter Σ, defined as

$$\Sigma = \varepsilon^{\beta}\sigma \qquad (6.2)$$

where $\beta > 0$ is as yet undetermined. Since when $m > 0$ we have that $I_{mn} \propto \exp\left(-(m\Sigma)^2\varepsilon^{2\beta}/2\right)$, terms with these coefficients are exponentially small in the asymptotic limit $\varepsilon \to 0$ at fixed Σ for any $\beta > 0$, and so the terms I_{0n} might be expected to dominate the behaviour. As a result, the expressions for I_{mn} can be simplified in the asymptotic limit, becoming

$$I_{mn} \sim \begin{cases} (n-1)!!\ \Sigma^n\ \varepsilon^{-n\beta} & m = 0 \text{ and } n \text{ even},\\ O(\exp[-\Sigma^2 m^2 \varepsilon^{-n\beta}/2]) & \text{otherwise.}\end{cases} \qquad (6.3)$$

m	$n=0$	$n=1$	$n=2$	$n=3$
0	1	0	σ^2	0
$m=\pm1$	$\mathrm{e}^{-\sigma^2/2}$	$\pm i\sigma^2\mathrm{e}^{-\sigma^2/2}$	$\sigma^2(1-\sigma^2)\mathrm{e}^{-\sigma^2/2}$	$\pm i\sigma^4(3-\sigma^2)\mathrm{e}^{-\sigma^2/2}$
$m=\pm2$	$\mathrm{e}^{-2\sigma^2}$	$\pm 2i\sigma^2\mathrm{e}^{-2\sigma^2}$	$\sigma^2(1-4\sigma^2)\mathrm{e}^{-2\sigma^2}$	$\pm i\sigma^4(6-8\sigma^2)\mathrm{e}^{-2\sigma^2}$
$m=\pm3$	$\mathrm{e}^{-9\sigma^2/2}$	$\pm 3i\sigma^2\mathrm{e}^{-9\sigma^2/2}$	$\sigma^2(1-9\sigma^2)\mathrm{e}^{-9\sigma^2/2}$	$\pm i\sigma^4(9-27\sigma^2)\mathrm{e}^{-9\sigma^2/2}$
$m=\pm4$	$\mathrm{e}^{-8\sigma^2}$	$\pm 4i\sigma^2\mathrm{e}^{-8\sigma^2}$	$\sigma^2(1-16\sigma^2)\mathrm{e}^{-8\sigma^2}$	$\pm i\sigma^4(12-64\sigma^2)\mathrm{e}^{-8\sigma^2}$

Table 1: Coefficients I_{mn} for the Gaussian kernel $K_G(x)$, for $|m|\leq 4$ and $0\leq n\leq 3$. $\pm$ signs in columns 1, 3 and 5 correspond to each other.

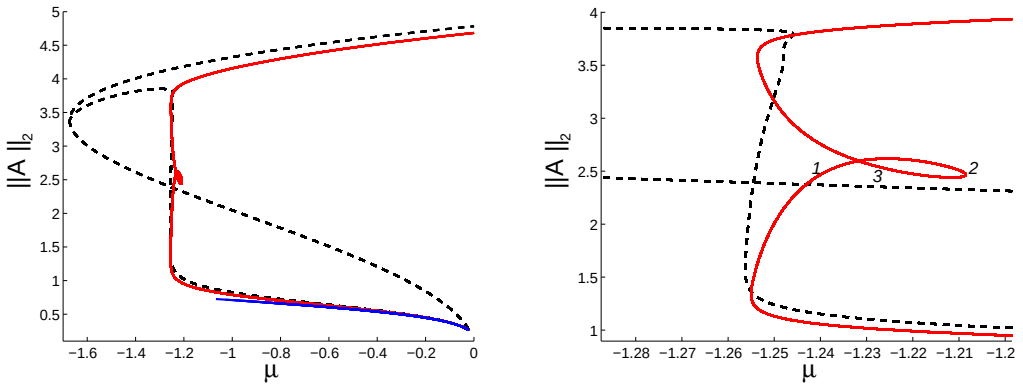

Figure 11: Left: Bifurcation diagram for solutions of the nonlocal Ginzburg-Landau equation (6.4) with a Gaussian kernel, for different values of the width parameter: $\Sigma=1$ (black, dashed), $\Sigma=2$ (red, solid) and $\Sigma=3$ (blue, solid, lowest curve). Right: enlargement of left-hand figure showing the additional 'loop' that arises in the $\Sigma=2$ case. Labels 1, 2 and 3 correspond to the profiles shown in figure 12. Other parameters are $\gamma=1.0$, $b_2=2.0$. The domain size $L=|\Omega|=20\pi$.

Substituting these limiting expressions into (6.1) we see that the order of successive terms in each of the summations is lowered from ε^{2n} to $\varepsilon^{(2-\beta)n}$. The coefficients in the series still rapidly become small since the factorial in the denominator grows more quickly than the double factorial in the numerator of each term.

There are two choices of β that allow the straightforward formation of a solvability condition at $O\left(\varepsilon^5\right)$. The first of these is the choice $\beta=1$ which leads to the amplitude equation

$$\begin{aligned} A_T &= \mu A+\frac{76}{9}b_0b_2A\left|A\right|^2+C_{10}A\left|A\right|^4+iC_8A_X\left|A\right|^2 \\ &\quad -\gamma\Sigma^2\left(\left|A\right|^2A_{XX}+2AA_X\bar{A}_X+A^2\bar{A}_{XX}\right)+4A_{XX}, \end{aligned} \tag{6.4}$$

where the coefficients b_0, C_8 and C_{10} are defined to be

$$\begin{aligned} b_0 &= \sqrt{\frac{27}{38}+\frac{18\gamma}{38}}, \\ C_8 &= \frac{16}{19}+\frac{32\gamma}{57}, \\ C_{10} &= -\frac{8820}{361}-\frac{7998}{361}\gamma-\frac{67415}{17328}\gamma^2. \end{aligned}$$

and b_2 is the departure from the codimension two point $b=b_0$, i.e. writing $b=b_0+\varepsilon^2b_2$ as in (5.12). The amplitude equation (6.4) is structurally distinct from (5.23) which was obtained in the narrow kernel case due to the presence of nonlinear cubic order terms involving two derivatives. In some sense the appearance of these new terms is balanced by a simplification of the dependence of the coefficients on the kernel function: in (6.4) the coefficients depend only γ and not on the rescaled width Σ.

Figure 11 illustrates three typical bifurcation diagrams obtained by continuation of solutions to (6.4). Solid and dashed lines do not indicate stability; they distinguish different parameter

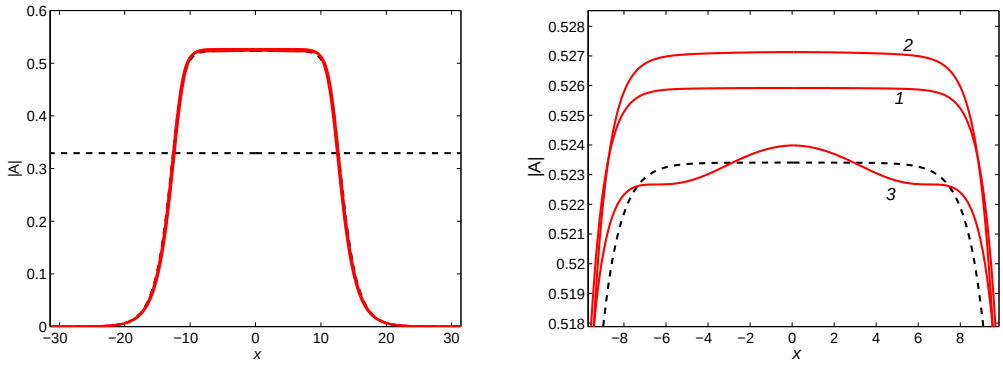

Figure 12: Left: Solution profiles for the nonlocal Ginzburg-Landau equation (6.4) with a Gaussian kernel, for different values of the width parameter: $\Sigma = 1$ (black, dashed), $\Sigma = 2$ (red, solid), all at $\|A\| = 2.5$. The horizontal line is the uniform solution Right: enlargement of left-hand figure showing the differences between the three solutions for $\Sigma = 2$ on the 'loop'. Continuing up the solid red curve in figure 11, increasing $\|A\|$ the profiles at $\|A\| = 2.5$ arise in the order: middle (1), top (2), lower (3). The black dashed curve is (as in the left-hand plot) for $\Sigma = 1$. Other parameters are $\gamma = 1.0$, $b_2 = 2.0$. The domain size $L = |\Omega| = 20\pi$.

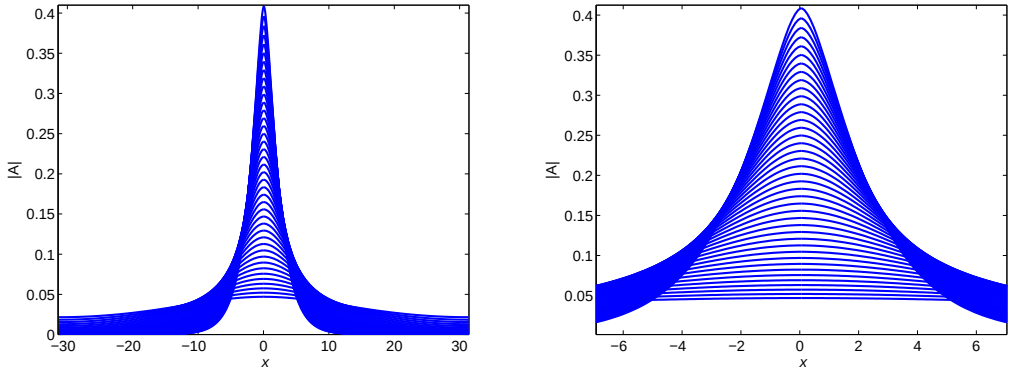

Figure 13: Left: Solution profiles for the nonlocal Ginzburg-Landau equation (6.4) with a Gaussian kernel for $\Sigma = 3$ along the lowest solution branch shown in figure 11. Right: enlargement of left-hand figure showing the evolution of the solutions near the point of blow-up. Other parameters are $\gamma = 1.0$, $b_2 = 2.0$. The domain size $L = |\Omega| = 20\pi$.

sets. The dashed black curves correspond to $\Sigma = 1$ and form the expected bifurcation diagram for the subcritical Ginzburg–Landau equation: there is a branch of uniform (constant) solutions that bifurcates subcritically and turns around at a fold bifurcation close to $\mu = -1.7$. A branch of spatially non-constant solutions bifurcates from the uniform branch near $\mu = 0$ and rejoins it near the saddle-node point. As the enlargement in figure 11(b) shows, in contrast to the case $\Sigma = 0$, this curve shows a small amount of hysteresis close to the nearly-vertical section. As Σ is increased to $\Sigma = 2$ (solid red curves) the branch of spatially non-constant solutions develops an intriguing additional loop in the centre of the 'nearly-vertical' section before extending into positive μ, without reconnecting to the spatially uniform branch at large amplitude. Solution profiles at $\|A\| = 2.5$, a value that cuts through the loop, are shown in figure 12. The profile becomes sharper, then develops additional undulations, as the loop is traversed starting from small-amplitude solutions. At larger amplitudes the solution resembles a sharp downwards-pointing spike embedded in a uniform, but non-zero, background state.

In general, it is not *a priori* clear that (6.4) remains well-posed as the amplitude of solutions $A(X)$ increases, due to the additional terms and the likelihood of singular behaviour for $\gamma\Sigma^2|A|^2 \approx 4$. This issue deserves detailed investigation, and we will return to it in future work. Its relevance to the formation of localised states is indicated by the (numerical) behaviour of solutions along the lowest (blue, solid) curve in figure 11. Solutions along this branch are shown in figure 13: solutions become increasingly sharp as their amplitude increases until numerical continuation fails

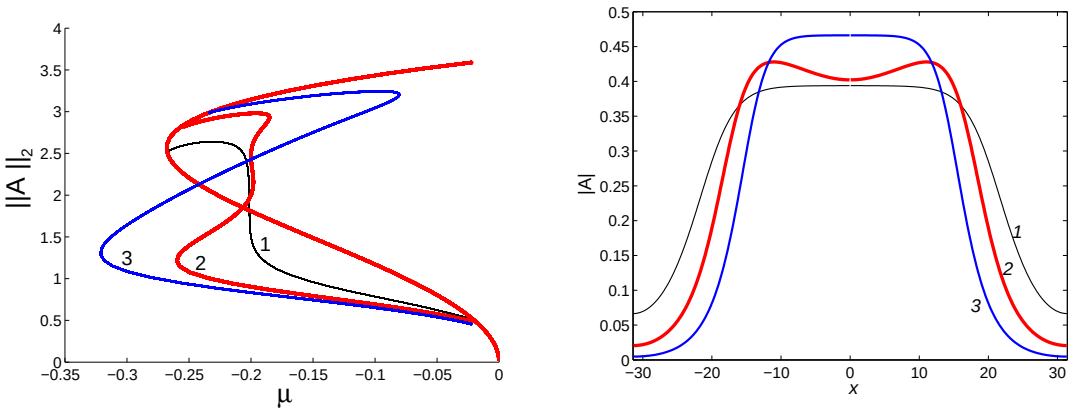

Figure 14: Left: Bifurcation diagram for solutions of the nonlocal Ginzburg-Landau equation (6.6) with a Gaussian kernel, for different values of the width parameter: $\Sigma = 0$ (black, labelled 1), $\Sigma = 3\pi$ (red, labelled 2) and $\Sigma = 10\pi$ (blue, labelled 3). Right: solution profiles for each curve of spatially modulated solutions at $\|A\|_2 = 2.5$, where the curves in (a) are close to intersecting. Note the central dip in the thick red curve (labelled 2). Other parameters are $\gamma_2 = 1.0$, $b_2 = 1.0$. The domain size $L = |\Omega| = 20\pi$.

to converge and the solution branch terminates. It is possible that this blow-up arises in a self-similar fashion.

The second natural distinguished limit that enables formation of a solvability condition at $O\left(\varepsilon^5\right)$ is the choice $\beta = 2$. In order to bring in the nonlocal terms at fifth order we combine this with a rescaling of the coefficient γ, writing $\gamma = \varepsilon^2\gamma_2$. In this distinguished limit the resulting envelope equation, again choosing a Gaussian kernel, is

$$\begin{aligned} A_T &= \mu A + \frac{76}{9}b_0 b_2 A|A|^2 - \frac{8820}{361}A|A|^4 + i\frac{16}{19}A_X|A|^2 \\ &\quad -2\gamma_2 A\sum_{n=1}^{\infty}\frac{(2n-1)!!}{(2n)!}\left(\Sigma D_X\right)^{2n}|A|^2 + 4A_{XX}, \end{aligned} \tag{6.5}$$

where again $b_0 = \sqrt{27/38}$. The choice $\beta = 2$ effectively makes the kernel act entirely on the long length scale X and so every term in the series expansion (6.1) at the same order in ε. Formally, the series expansion is equivalent to the integral term, so that a more compact way of writing the amplitude equation is

$$\begin{aligned} A_T &= \mu A + \frac{76}{9}b_0 b_2 A|A|^2 - \frac{8820}{361}A|A|^4 + i\frac{16}{19}A_X|A|^2 \\ &\quad -2\gamma_2\int_\Omega \mathrm{e}^{-(X-Y)^2/(2\Sigma^2)}|A(Y)|^2\,dY + 4A_{XX}. \end{aligned} \tag{6.6}$$

This nonlocal Ginzburg–Landau equation captures the nonlocal dynamics sufficiently strongly to reproduce aspects of the stretched and slanted snaking behaviour apparent in figures 3 and 4. Figure 14 contains bifurcation diagrams and solution profiles for three choices of Σ, moving from the purely local problem ($\Sigma = 0$, thin black curve) to nearly the global one ($\Sigma = L/2$, medium thickness blue curve). For each value of Σ in figure 14(a), the curves of uniform constant solutions for $|A|$ are almost exactly superposed: of these only the thickest (red) curve is visible. The thin black line for the $\Sigma = 0$ case has a near-vertical central section, just as in figure 2. The thick red curve indicates how this vertical curve is deformed as the width of the nonlocal kernel is increased: the lower part moves to the left and the upper part to the right. This is exactly the behaviour observed for the homoclinic snaking in figures 4. The central section remains very close to the central section in the case $\Sigma = 0$. As the kernel width increases further we approach, smoothly, the slanted snaking limit in which the curve assumes its characteristic 'Z' shape. This transition takes place monotonically and smoothly, in contrast to the many disconnection and reconnection events associated with the homoclinic snaking curves themselves, and illustrated, for the top hat kernel, in figures 5 and 6. Figure 14(b) shows solution profiles $|A(X)|$ on the three bifurcation curves in 14(a) at points close to where all three curves of spatially modulated solutions intersect. We see that the thickest (red) curve for intermediate kernel widths contains a central trough and off-centre peaks that are not present in the other two cases. This indicates the propensity of localised

states for these intermediate kernel widths (more precisely, kernel widths that are longer than the basic wavelength of the pattern forming instability yet shorter than the width of the domain) to prefer to form multipulse states rather than single-pulse states. This therefore goes a little way towards justifying the collisions between the primary snaking curves and those of multipulse states described in figures 5 and 6.

7 Conclusions

In this paper we have considered equilibrium solutions, in the form of spatially localised states, to the one dimensional Swift–Hohenberg equation extended by a nonlocal term in convolution form. Numerical results suggested that the well known 'homoclinic snaking' structure was deformed and perturbed in several different ways as a result of the presence of nonlocality. We focussed our analytical efforts on extending the multiple-scales analysis for the Swift–Hohenberg equation to cope with the nonlocal term. Through (formal) expansions and application of Fourier transforms we were able to reduce the nonlocal integrodifferential Swift–Hohenberg equation into one of three Ginzburg–Landau-type equations that applied in different distinguished limits. These different limiting equations captured different aspects of the problem. As a direction for future work it would be of interest to link the results of Kao and Knobloch [18], which concern the behaviour of solutions to the cubic-quintic Ginzburg–Landau equation, to the parameter dependencies of the coefficients that the nonlocal terms produce.

While we focussed on two particular kernels, the 'top hat' composition of Heaviside step functions, and a Gaussian kernel, we present analytic results in as much generality as possible, writing the coefficients in the Ginzburg–Landau equations in terms of the Fourier transform of the kernel function. The Gaussian case can be motivated straightforwardly in applications since the convolution term is the solution of the initial value problem for the diffusion equation. The nonlocal term could then be thought of as directly modelling the diffusive spread of the solution, through interaction with another physical quantity, such as temperature, over timescales short compared to the time evolution of the Swift–Hohenberg equation itself.

On the mathematical side, it would be useful and interesting to extend results obtained recently by Achleitner and Kuehn [2] on the persistence of solutions in the presence of convolution terms, to prove that for kernels that are sufficiently narrow the homoclinic snaking bifurcation structure persists. Numerical work to investigate exactly the sequence of collisions with multipulse states for a specific choice of kernel would also be of interest.

Moreover, it would be desirable to extend the analysis of this one dimensional problem to two or three space dimensions, clearly of substantial physical relevance. There is plenty of room for optimism since Fourier transform results often extend easily to higher dimensions, so that such extensions may be achievable with largely similar techniques to those presented here. These and many other considerations in this complex problem are left to be the subject of future work.

Acknowledgements

JHPD gratefully acknowledges the support of the Royal Society through a University Research Fellowship.

References

[1] M. Abramowitz and I.A. Stegun, *Handbook of Mathematical Functions with Formulas, Graphs, and Mathematical Tables*. US. Nat. Bureau of Standards (1964)

[2] F. Achleitner and C. Kuehn. On bounded positive stationary solutions for a nonlocal Fisher–KPP equation. Preprint. arXiv: 1307.3480 (2013)

[3] D. Avitabile, D.J.B. Lloyd, J. Burke, E. Knobloch and B. Sandstede, To snake or not to snake in the planar Swift-Hohenberg equation. *SIAM J. Appl. Dyn. Syst.* **9**, 704–733 (2010)

[4] J. Burke and E. Knobloch, Localized states in the generalized Swift–Hohenberg equation. *Phys. Rev.* E **73**, 056211 (2006)

[5] J. Burke and J.H.P. Dawes, Localised states in an extended Swift–Hohenberg equation. *SIAM J. Appl. Dyn. Syst.* **11**, 261–284 (2012)

[6] A. Champneys, Homoclinic orbits in reversible systems and their applications in mechanics, fluids and optics. *Physica* D **112**, 158–186 (1998)

[7] S.J. Chapman and G. Kozyreff, Exponential asymptotics of localised patterns and snaking bifurcation diagrams. *Physica* D **238**, 319–354 (2009)

[8] S. Coombes, G.J. Lord and M.R. Owen, Waves and bumps in neuronal networks with axo-dendritic synaptic interactions. *Physica* D **178**, 219–241 (2003)

[9] P. Coullet, C. Riera and C. Tresser, Stable static localized structures in one dimension. *Phys. Rev. Lett.*/ **84**, 3069–3072 (2000)

[10] M. Cross and H. Greenside, *Pattern Formation and Dynamics in Nonequilibrium Systems*. CUP, Cambridge (2009)

[11] J.H.P. Dawes, The emergence of a coherent structure for coherent structures: localized states in nonlinear systems. *Phil. Trans. R. Soc. Lond.* A **368**, 3519–3534 (2010)

[12] J.H.P. Dawes and H. Susanto, Variational approximation and the use of collective coordinates. *Phys. Rev.* E **87**, 063202 (2013)

[13] A.D. Dean, P.C. Matthews, S.M. Cox and J.R. King, Exponential asymptotics of homoclinic snaking. *Nonlinearity* **24**, 3323-3351 (2011)

[14] E.J. Doedel, A.R. Champneys, T. Fairgrieve, Y. Kuznetsov, B. Oldeman, R. Paffenroth, B. Sandstede, X. Wang and C. Zhang, AUTO-07p: continuation and bifurcation software for ordinary differential equations. Available online at `http://indy.cs.concordia.ca/auto/` (2011)

[15] W.J. Firth, L. Columbo and A.J. Scroggie, Proposed resolution of theory-experiment discrepancy in homoclinic snaking. *Phys. Rev. Lett.* **99**, 104503 (2007)

[16] R.B. Hoyle, *Pattern Formation: An introduction to methods*. CUP, Cambridge (2006)

[17] A. Hutt and F.M. Atay, Analysis of nonlocal neural fields for both general and gamma-distributed connectivities. *Physica* D **203**, 30–54 (2005)

[18] H.-C. Kao and E. Knobloch, Weakly subcritical stationary patterns: Eckhaus instability and homoclinic snaking. *Phys. Rev. E* **85**, 026207 (2012)

[19] G. Kozyreff and S.J. Chapman, Asymptotics of large bound states of localized structures. *Phys. Rev. Lett.* **97**, 044502 (2006)

[20] E.H. Lieb and M. Loss, *Analysis*. Graduate Studies in Mathematics Volume 14, Second Edition. AMS, Providence. (2010)

[21] P.C. Matthews and H. Susanto, Variational approximations to homoclinic snaking in continuous and discrete systems. *Phys. Rev.* E **84**, 066207-11 (2011)

[22] E. Plaut and F.H. Busse, Low-Prandtl-number convection in a rotating cylindrical annulus. *J. Fluid Mech.* **464**, 345–363 (2002)

[23] H.-G. Purwins, H.U. Bödeker and S. Amiranashvili, Dissipative solitons. *Adv. Phys.* **59**, 485–701 (2010)

[24] H. Susanto and P.C. Matthews, Variational approximations to homoclinic snaking. *Phys. Rev.* E **83**, 035201(R) (2011)

[25] C. Taylor and J.H.P. Dawes, Snaking and isolas of localised states in bistable discrete lattices. *Phys. Lett.* A **375**, 14–22 (2010)

[26] U. Thiele, A.J. Archer, M.J. Robbins, H. Gomez and E. Knobloch, Localized states in the conserved Swift-Hohenberg equation with cubic nonlinearity, *Phys. Rev.* E **87**, 042915 (2013)

[27] J. Vega, Instability of the steady states of some Ginzburg–Landau-like equations with real coefficients. *Nonlinearity* **18**, 1425–1441 (2005)

[28] N.A. Venkov, S Coombes and P.C. Matthews, Dynamic instabilities in scalar neural field equations with space-dependent delays, *Physica* D **232**, 1–15 (2007)

[29] P.D. Woods and A.R. Champneys, Heteroclinic tangles and homoclinic snaking in the unfolding of a degenerate reversible Hamiltonian–Hopf bifurcation. *Physica* D **129**, 147–170 (1999)